Modeling of Cell Migration Assays Including Electrotaxis

Undergraduate Honors Thesis

Anu Kaushik

Advisor: Dr. Vish Subramaniam

Department of Mechanical and Aerospace Engineering

The Ohio State University

Spring 2014

Abstract

Cell motility is important in embryonic development, wound-healing, and the metastasis of cancer. There are different stimuli that guide cell motility in biological tissue. One of these stimuli is electrical in nature (the others being chemical and mechanical), and the mobility of cells under the presence of electric fields is called electrotaxis. It is well known that potential differences on the order of 20mV to 50mV exist across epithelial tissue. It is also known that when epithelial tissue is compromised resulting in a wound, a short circuit is created across the basement membrane. This endogenous electric field drives a flow of electrical current and cells towards the more negative site of the wound, driving closure. If bioelectricity plays an important role in moving cells in specific directions, then increasing the strength of the electric field and varying its direction *in vivo* can either accelerate or decelerate cell movement as desired. Bioelectricity therefore offers the possibility of controlling and potentially accelerating wound-healing or retarding the metastasis of cancer. Conventional methods of studying and inducing electrotaxis have involved the use of metal electrodes placed in contact with the tissue or medium containing cells using agar salt bridges. This approach raises the possibility of contamination as well as unwanted effects of Ohmic heating. In this research, electric fields are induced *in vitro* in a non-contact manner, thereby eliminating any interfering electrochemical interactions or unwanted heating arising from flow of direct current through the culture medium. The goal of this research is to quantify and simulate cell movement in a standard wound-healing assay using numerical methods to solve the relevant two-dimensional transient governing equations. Preliminary results have been obtained from non-contact electrotaxis experiments, and a time-varying 2-D model has been developed that simulates and can eventually predict the migration of cells in response to an electrical stimulus. This model can be useful for further studies delving into mechanisms driving electrotaxis. Moreover, this work may lead to development of non-invasive means of treating patients with chronic wounds or burns or halting metastasis.

Table of Contents

List of Figures

4

List of Tables

Chapter 1

Introduction

1.1) Historical Background

Cell motility is important in embryonic development, wound healing, and the metastasis of cancer. There are various stimuli (mechanical, chemical, and electrical) that guide the motility of cells in biological tissue. The movement of cells in the presence of electric fields is called electrotaxis (also known as galvanotaxis). The term galvanotaxis is coined after Luigi Galvani, who in the 1780s, while performing experiments on frogs at the University of Bologna, is famously known to have accidentally touched a frog's leg with two dissimilar metal electrodes. The electrodes generated an applied electric field and current flow, which immediately caused the dead frog to twitch[1]. Figure 1 illustrates Galvani's realization of "animal electricity," a term he used to describe the concept of bioelectricity.
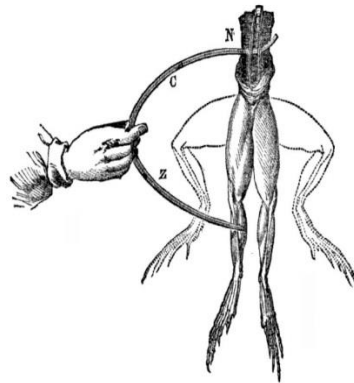
Figure 1: Luigi Galvani's frog twitch experiments in the 1780's [1]

1.2) Electrotaxis

Galvani's experiment was the first one to explore the idea of bioelectricity. Since then, researchers have discovered the existence of voltage potentials on the order of 20mV to 50mV across epithelial tissue (Figure 2). It is also known that a wound in the form of a cut in the epithelial tissue results in an electrical short across the basement membrane which normally separates charges between epithelial layers and the underlying connective tissue and stroma. This potential gradient then drives an electric current flow towards the more negative site – the wound [1]. If bioelectricity plays an important role in moving cells in a specific direction, then

increasing the strength of the electric field *in vivo* artificially can either accelerate cell movement (as in the case of wound-healing) or decelerate cells (as in cancer metastasis) as desired. Electrotaxis therefore offers the possibility of controlling and potentially accelerating wound healing or retarding the metastasis of cancer.
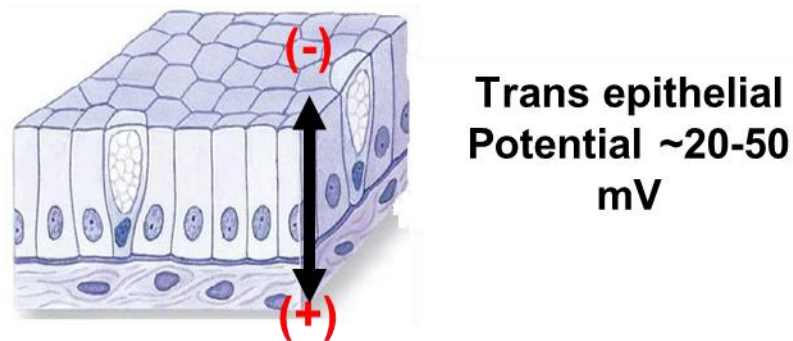
Figure 2: Potential difference between epithelial surface and basement membrane [2]

1.3) Literature Review

The directional movement of cells in the presence of electric fields has been observed by numerous researchers. Foulds and Barker [3] were able to show the existence of a "skin battery" experimentally by measuring potentials on the order to 20mV to 50mV across the dermis at various sites of the body for seventeen humans. Nishimura, Isseroff, and Nuccitelli [4] showed that human keratinocytes respond directionally in the presence of an electric field of greater strength than 5mV/mm.

Despite the observations made about cell movement in the presence of electric fields, the scientific community is yet to fully understand the mechanisms underlying this phenomenon. Pullar, Isseroff, and Nuccitelli [5] were able to show the importance of kinase signaling pathways in cells in directing keratinocyte electrotaxis. Upon inhibition of the protein kinase, a significant reduction in electrotactic response was observed. Zhao [6] further probed the cellular mechanisms involved in cell movement and how electric fields may be having an effect on the specific signaling pathways in cells. It was proposed that in the presence of electric fields, polarized membrane lipid domains and EGF receptors may cause asymmetrical signaling through kinase, triggering a directional cellular movement response

There is great potential for electrotaxis to be leveraged clinically, and several attempts have been made to develop products for faster wound healing. Chu et al. [7] explored the effects

7

of dressing wounds with silver-nylon bandages that drive small currents to stimulate electrotaxis. Vomaris [8] is a company that strives to make bandages called Procellera that are coated with patterned regions of silver oxide and zinc to generate an electric field in the presence of a wound [9].

All of the experiments performed to study electrotaxis to date have involved direct contact of electrodes with the culture medium containing the cells. Huo et al. [10] looked to induce electric fields on the order of 2.5mV/cm onto human keratinocytes and fibroblasts for the first time non-invasively using a Field Therapy Accelerator. More recent work by Sequin et al. describes a method of applying electric fields to a conducting cell media without direct contact using an electromagnetic coil [11]. The experimental results from keratinocytes and highly metastatic breast cancer cells in this work form the starting point for the model developed in this research. Kostic, Lynch, and Sheetz [12] describe the effect of cellular microenvironment on metastasis. A highly metastatic breast cancer cell line, SCP2, that is observed in this work is the specific cell line used in ref. [11] in addition to an immortalized cell line of human keratinocytes.

Since the work presented in this thesis primarily focuses on developing a model to characterize cell behavior, several similar models were explored to understand the possible range of physical solutions. R.A. Fisher's [13] paper on solving the traveling wave equation in order to track propagating fronts of a population, given a gene mutation, formed the basis of the parametric relationships used in this work. The reaction diffusion equation, and its application to solve a variety of biological problems, is further explored in the work of Volpert and Petrovskii [14]. Vanegas-Acosta et al. [15] considered cell movement of osteoblasts in a very different assay geometry than the one utilized in this research, but this model nonetheless serves as a point of comparison for the model developed in this research.

This thesis is organized as follows. The following chapter provides the motivation and objectives for the work presented in this paper. The experimental setup and procedure are discussed in Chapter 3. Preliminary results from the experiments are summarized in Chapter 4. The development of the model based on the experiments is the focus of Chapter 5. Chapter 6 expands the model to two dimensions and discusses the procedure for solving the governing equations. Chapter 7 details the results from simulations of the model. Finally this thesis is summarized thereafter, followed by recommendations for future work.

Chapter 2

Motivation and Objectives

2.1) Motivation

Electrotaxis initiated by application of an externally applied electric field offers the possibility of accelerating or decelerating cells as desired. However, more work needs to be done to characterize this phenomenon in order to facilitate its application in a clinical setting. Conventional experiments that study the motion of cells in the presence of electric fields follow a setup as shown in Figure 3 that include a cell culture in indirect contact to electrodes via an agar salt bridge [1]. Despite the remoteness of the electrodes, various electrochemical contaminants (i.e. ions) may be introduced into the cell culture via the agar bridges. In addition, there may be adverse effects due to Ohmic heating present in the experiment since the current flow may be constricted depending on the path of least resistance followed. The indirect contact, therefore, does not allow for an isolated study of electrotaxis, free from spurious effects. It is beneficial to study the movement of cells, therefore, in the presence of an electric field applied without contact. Since such a scheme would require the electric field to be applied inductively and therefore cannot be measured directly, it is necessary to develop a model of the process as well.
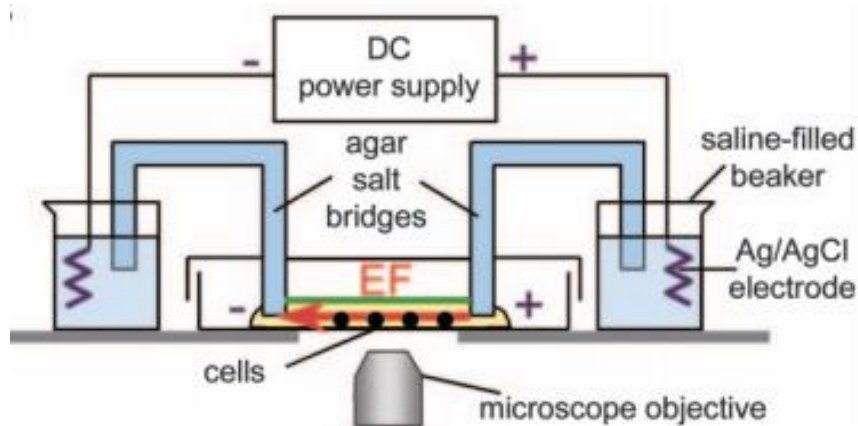
Figure 3: Conventional electrotaxis experimental setup [1]

A model is a useful way for quantifying the results from an experimental assay. It is a useful tool for researchers to compare changes across control cases in light of the many external factors that may affect an experimental setup including cell culture differences and other environmental variables. Moreover, a robust model can be used as a predictive means to

optimize further experimental work. To the best of this author's knowledge, there are few references in the literature [15] that develop such a model, and none have been developed for cell migration assays based on the relevant physics. Moreover, expanding such a model to include the effect of applied electric fields on cells can be a very useful tool to further understand the phenomenon of electrotaxis.

2.2) *Objectives*

The idea of applying electric fields in a non-contact manner to induce cell motility has been recently described by Sequin et al. [11]. In their work, an electric field is applied to a cell culture inductively using a coil through which a time-varying current is driven. Preliminary results from this work are presented in this thesis, and these results are used as a starting point for developing a model.

In following the experiments performed by Sequin et al. [11], the primary goal of this research is to develop a time varying, two-dimensional model that mimics the observations of the cells in these experiments. The relevant physical equations must be obtained that describe the movement of cells, and a two-dimensional governing equation or equations must be developed to describe cellular movement. Ultimately, a time-lapse simulation of the experiment must be developed that can be used to quantify and eventually predict cell motility.

A secondary goal of this work is to incorporate the effect of electric fields on cellular motion into the model. A plausible theory must be developed to describe the physics of electrotaxis, and this must be incorporated into the model. Finally the model must be tested for validity across experiments.

Chapter 3

Experimental Apparatus

3.1) Wound-Healing Assay

The idea of applying electric fields in a non-contact manner is recent [10] [11]. A time varying magnetic field is applied to a culture dish containing keratinocytes cultured in standard DMEM media [11]. The medium containing the cells is electrically conducting; therefore, the time varying magnetic field induces an electric field in the medium, by Faraday's Law. This induced electric field drives (or inhibits) cell motility. The experimental setup is illustrated in Figure 4.
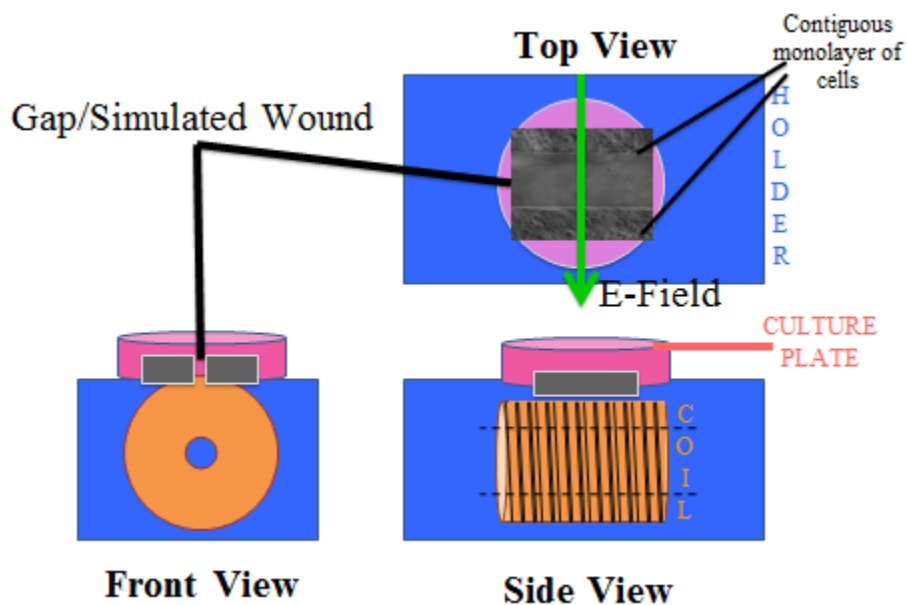
Figure 4: Schematic of experimental apparatus for wound healing assay [11]

The time varying magnetic field is applied by an in-house designed electromagnet placed under the culture plate containing the cells in the medium. An alternating current is passed through the coil, which then results in the time varying magnetic field, through Ampère's Law. Figure A1 in Appendix A further illustrates the electromagnetic principles underlying the non-contact application of an electric field.

The first experiment presented in this work was performed on an immortalized cell line of human keratinocytes. For this experiment, a contiguous layer of cells was placed in the culture

plate. A well-defined rectangular region in the middle, devoid of cells, simulated the wound. The specific culture insert used in this assay is shown in Figure A2 of Appendix A. The approximate width of this particular gap was about 500μm. A 1Hz, 20V peak-to-peak sawtooth voltage waveform was applied across the coil, which then resulted in a 1Hz sawtooth current (Figure 5). Control experiments were conducted on the same assay but without any applied electromagnetic field. The cell culture was imaged on a phase contrast microscope every 4 hours, digitized, and the exposed area of the simulated wound was calculated by numerical integration after importing the digitized data into MATLAB.
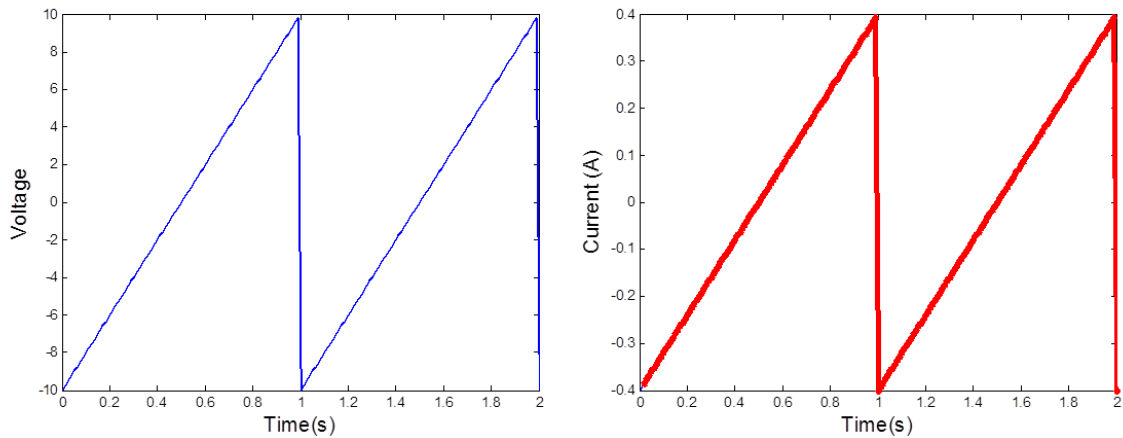
Figure 5: Input voltage and resulting current

The second experiment presented in this work was performed on SCP2 cells, which are a highly metastatic breast cancer cell line [12]. For this experiment, an 80% confluent layer of cells was placed in the culture plate. The tip of a pipette was used to introduce a scratch through the middle of the cell culture. The approximate width of this particular gap was about 1.1mm. A 100kHz sawtooth voltage waveform was then passed through the coil. Images from this experiment were gathered in the same way as the previous experiment.

3.2) Electromagnetic Coil

The coil used for both experiments described in the previous section was referred to as H1 for its sequence in the design and construction process in the Applied Physics Laboratory. H1 uses copper wire of radius 0.268mm (23 AWG). The coil is 2.47cm long with an inner radius of 0.71cm and outer radius of 2.33cm. There are 18 layers of windings in the coil, with 87 turns per layer. The coil was measured to have a resistance of 25Ω and an inductance of 12.1mH.

Chapter 4

Preliminary Experimental Results

4.1) Keratinocyte (HaCaT Cells)

For the experiment with keratinocyte cells, over eight hours, it was found that the cell fronts closed significantly less compared to the control. Thus, gap closure was *inhibited* in the presence of an electric field. This is shown in the images in Figure 6. Figure 7 then quantifies the percentage of gap closure over time. Gap closure here refers to the percentage of the original gap area that is filled with cells after the experiment begins. The gap closure values were obtained after digitizing the microscope images from Figure 6, and numerically integrating the area of the gap in MATLAB. From Figure 7, it may be qualitatively noted that the time rate of change of gap closure for this experiment is nearly constant.
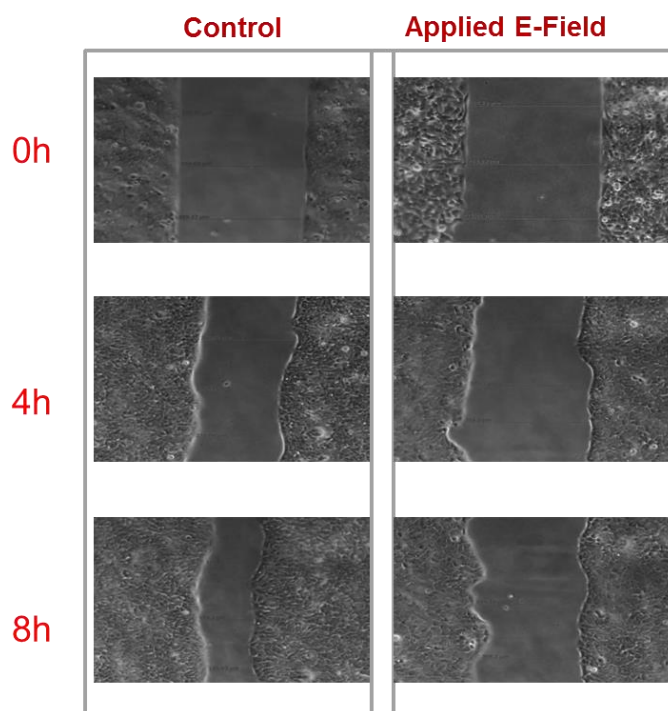
Figure 6: Results from wound healing assay with keratinocytes
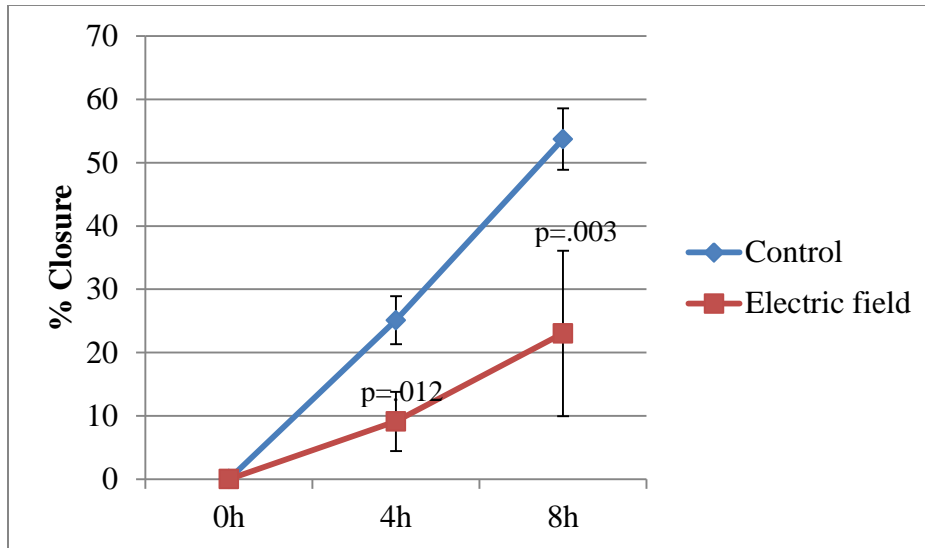
Figure 7: Keratinocyte closure over time with and without an induced electric field

4.2) Highly Metastatic Breast Cancer Cells (SCP2)

For the experiments with the highly metastatic breast cancer (SCP2) cells, over sixteen hours, it was found that the cell fronts closed less with the induced electric field compared to the control. Thus, as in the results of the experiments with Keratinocytes, gap closure was once again *inhibited* in the presence of an electric field. This is shown in Figure 8. Figure 9 then quantifies the percentage of gap closure over time. Gap closure here refers to the percentage of the original gap area that is filled in with cells at the end of the experiment.
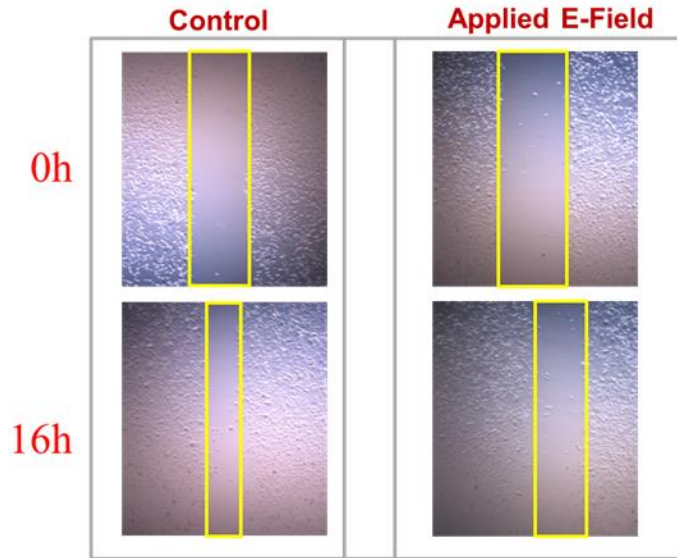
Figure 8: Results from wound healing assay with SCP2 cells
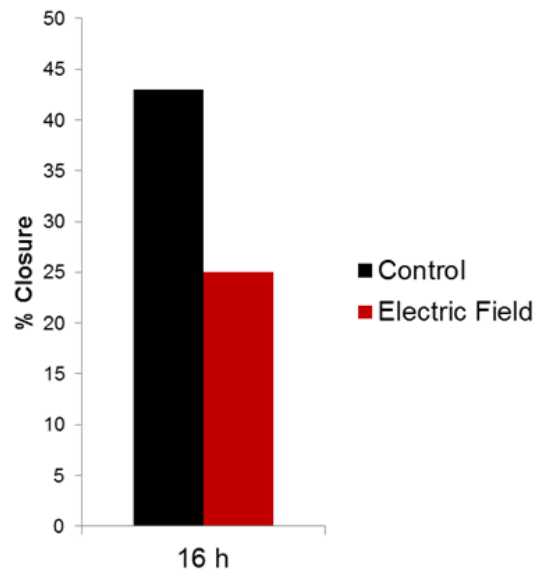
Figure 9: SCP2 closure over time with and without an induced electric field

Chapter 5

Development of Model

5.1) Control Volume Analysis

It is not only important to show the effect of electric fields on cell motility experimentally, but it is imperative to quantify and eventually be able to predict cellular motion in these wound-healing assays. This can be done by developing a model that mimics the behavior of cells in the assay. Such a model can then be used to optimize subsequent electrotaxis experiments and may even prove useful for predictive purposes.

A control volume approach was utilized to develop a model for cellular motion in the wound-healing assay. First, a control volume is placed in the simulated wound (Figure A3 of Appendix A). Some simplifying assumptions are then made about the cells in the control volume:

1. The cells are assumed to exist as a contiguous monolayer
2. The number of cells per unit volume (or area) or cell number density is taken to be a continuous variable

Next, the flux of cells through the control volume in one dimension can be described as shown in Figure 10:
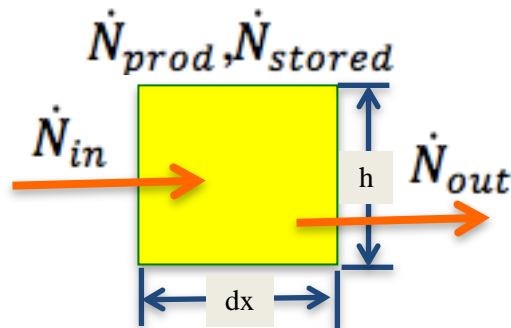
Figure 10: Flux through the control volume in 1-dimension

Here, $\dot{N}$ is the number flow rate of cells, and the various flow rates can be defined as follows:

$$\dot{N}_{in} = nV(h)(1) \tag{1}$$

where n describes the number density of cells traveling at some velocity V. Next, the number flow rate going out can be described using a first-order Taylor Series expansion:

$$\dot{N}_{out} = nV(h)(1) + \frac{\partial}{\partial x}(nV)(h)(1)dx \tag{2}$$

The number flow rate stored is the time rate of change of cells in the control volume:

$$\dot{N}_{stored} = \frac{\partial}{\partial t}(n)(h)(1)dx \tag{3}$$

Finally, the net rate of production (proliferation) of cells under competition for limited resources can be taken into account. Cell replication here is taken to be proportional to the number density n, and to the available resources.

$$\dot{N}_{prod} = sn(n_\infty - n)(h)(dx)(1) \tag{4}$$

s is the rate coefficient for cell production and is taken to be a constant. n_∞ is the steady-state cellular number density far away from the simulated wound. The expression $sn(n_\infty - n)$ used here follows a logistic growth pattern, and is often used to characterize cell population growth in the presence of limited resources [14].

It is now possible to combine the flow rates using the conservation of mass or in this case conservation of a single species:

$$\dot{N}_{in} + \dot{N}_{prod} = \dot{N}_{out} + \dot{N}_{stored} \tag{5}$$

When combined, like terms cancel out to yield the following equation:

$$\frac{\partial n}{\partial t} + \frac{\partial}{\partial x}(nV) = sn(n_\infty - n) \tag{6}$$

where V is a diffusion velocity for the cells, which is taken here to be given by a constitutive equation such as Fick's Law:

$$nV = -\mathcal{D}\frac{\partial n}{\partial x} \tag{7}$$

where $\mathcal{D}$ is a diffusivity describing cell migration in the absence of any external forces. Substituting Equation 7 into Equation 6 yields:

$$\frac{\partial n}{\partial t} = \mathcal{D}\frac{\partial^2 n}{\partial x^2} + sn(n_\infty - n) \tag{8}$$

This equation is a non-linear diffusion equation and reduces to the standard linear diffusion equation encountered in many branches of physics and engineering when $s = 0$.

The parameters that appear in Equation 8 are listed in Table 1 along with their definitions and units.

Table 1: Understanding the parameters

Parameter	Units	Description
n	$[\text{cells/m}^3]$	Cell number density (dependent variable)
$\mathcal{D}$	$[\text{m}^2/\text{s}]$	Average diffusion coefficient for cellular motion
s	$[\text{m}^3/\text{s}]$	Rate coefficient for production of cells under competition for resources
n_∞	$[\text{cells/m}^3]$	Cell number density far away from the gap

The sections below describe the roles of the individual parameters in special cases of the one-dimensional governing equation, and Section 6.5 later shows how initial estimates were obtained for these parameters based on the experimental results.

5.2) *Special Cases of Non-linear Reaction-Diffusion Equation*

Before delving into the complexity of finding solutions for the governing equation (Equation 8), it is instructive to consider certain special cases of the equation. These special cases can provide insights into the roles of the individual parameters s, $\mathcal{D}$, and n_∞. These insights can later be used in solving the relevant two-dimensional case of the governing equation. The MATLAB scripts for obtaining the solutions in all of the cases described next are given in Appendix C

18

5.2.1)   *Spatially Homogeneous Case*

The first case to consider is the special case of spatial homogeneity, when there is no variation in relation to x. The governing one-dimensional partial differential equation can be then condensed into the following ordinary differential equation:

$$\frac{dn}{dt} = sn(n_\infty - n) \tag{9}$$

It is useful to consider the non-dimensional form of the differential equation for a better understanding of the parameters. Letting $\bar{n} = \frac{n}{n_\infty}$, the following non-dimensionalized equation is obtained:

$$\frac{d\bar{n}}{dt} = sn_\infty \bar{n}(1 - \bar{n}) \tag{10}$$

For this particular ordinary differential equation, an analytical solution may be obtained, assuming some initial value n_i for cellular number density. The steps involved in acquiring the following analytical solution are given in Appendix B.

$$\bar{n} = \frac{1}{1+\left(\frac{n_\infty}{n_i}-1\right)e^{-sn_\infty t}} \tag{11}$$

The solution for $\bar{n}$ as given by Equation 11 is shown in Figure 11.
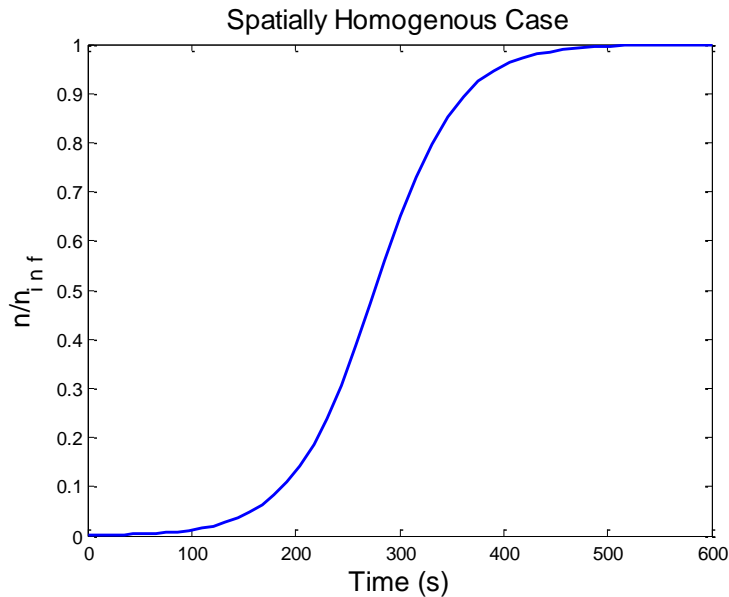
Figure 11: Spatially homogeneous logistical growth, s = 1x10^{-9} m^3/s

Figure 11 shows the net production of cells through replication until some steady state value, n_∞ is reached. The parameter s also takes into account cellular competition for limited resources. The plot follows a logistic growth pattern [16], a model that is frequently used to describe population growth and even cellular dynamics and tumor growth [14]. The parameter s represents a time constant that dictates cellular growth to steady state. Generally, a larger value of s indicates a faster cellular growth rate.

5.2.2)   *Steady State Case*

For the steady state special case, $\frac{\partial n}{\partial t}$ is set to 0 to yield the following differential equation:

$$-\mathcal{D}\frac{d^2 n}{dx^2} = sn(n_\infty - n) \tag{12}$$

Letting $\bar{n} = \frac{n}{n_\infty}$ and letting $\bar{x} = \frac{x}{L_{eff}}$ where L_{eff} can be considered to be the diameter of the culture dish (5cm), Equation 13 can be non-dimensionalized to yield:

$$-\frac{\mathcal{D}}{L_{eff}^2}\frac{d^2\bar{n}}{d\bar{x}^2} = sn_\infty\bar{n}(1 - \bar{n}) \tag{13}$$

The resulting equation is solved numerically and displayed in Figure 12. As can be seen in Figure 12, there is a strong relationship between the parameters s and $\mathcal{D}$ that dictate the shape of the graph or even the existence of a solution.
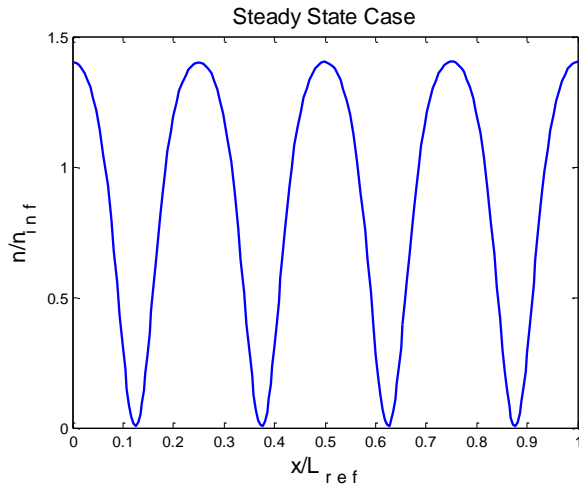
Figure 12: Steady state striations, s/D = 3/1, $\mathbf{n_\infty \gg n}$

20

The resulting oscillations in the plot in Figure 12 is obtained if $n_\infty \gg n$. A sinusoidal solution here is expected as the $(1 - \bar{n})$ drops out in the differential equation and is overpowered by the linear $s n_\infty \bar{n}$ term. The solution may actually describe a physical solution, wherein the cells form striations in the culture plate. Figure 13 illustrates this special case of oscillating cell number densities along the horizontal axis. It is not known whether or not this is physically realizable experimentally.
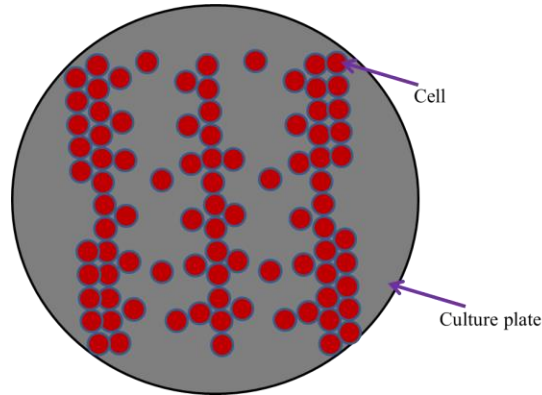
Figure 13: Striations in a cell culture plate

The steady state special case may also be considered for $n_\infty \approx n$. Such a case yields much more volatile solutions, one of which is shown in Figure 14.
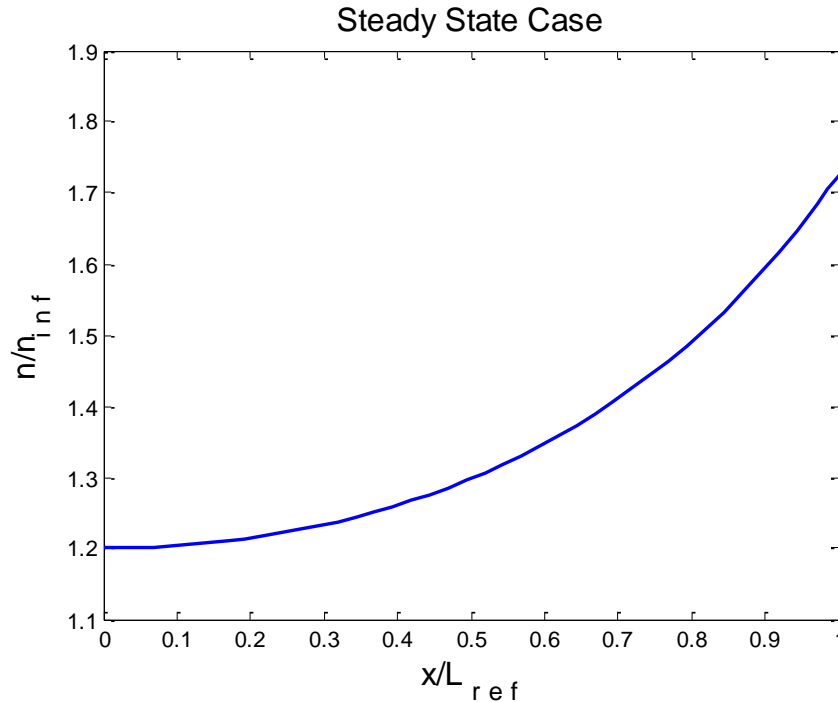
Figure 14: Steady state case where $n_\infty \approx n$, s/D = 3/1

5.2.3) *Traveling Wave*

The Fisher-Kolmogorov equation is a special one-dimensional case of the reaction-diffusion equation (Equation 8). In 1937, R.A. Fisher considered the case of population dynamics, given a gene mutation. He sought a solution to the following equation that has a linear source term [13]:

$$\frac{\partial p}{\partial t} = k\frac{\partial^2 p}{\partial x^2} + mpq \qquad (14)$$

Here, p is the dependent variable, analogous to n in the model for the migration assay. k in Equation 14 is analogous to diffusivity, and m is used in a very similar way to the rate coefficient for production of cells under competition for resources s. q in Fisher's equation is the frequency of the parent allelomorph, and is analogous to n_∞. In his analysis, Fisher proposed a solution that describes traveling waves of constant velocity that propagate through space over time (Figure 15).
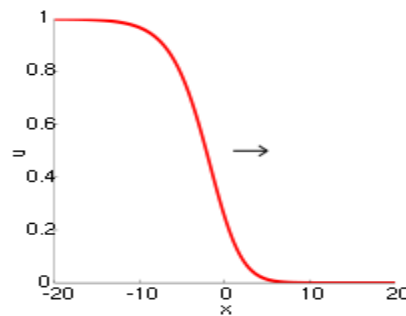
Figure 15: A traveling wave front using Fisher's approach. Here some dependent variable u is plotted as a function of x captured at some particular time step. Source: en.wikipedia.org [17]

Using Fisher's approach, it is useful to consider the cell fronts in the assay closing inwards at some constant velocity u. It is then possible to make the following substitution into the governing differential equation:

$$\frac{\partial n}{\partial t} = -u\frac{\partial n}{\partial x} \qquad (15)$$

Substituting Equation 15 into the governing partial differential Equation 8 leads to a second order ordinary differential equation:

$$\mathcal{D}\frac{d^2n}{dx^2} + u\frac{dn}{dx} = -sn(n_\infty - n) \tag{16}$$

Equation 16 can also be non-dimensionalized in the same way as was performed in the previous sections to yield:

$$\frac{\mathcal{D}}{L_{eff}^2}\frac{d^2\bar{n}}{d\bar{x}^2} + \frac{u_{ref}}{L_{eff}}\bar{u}\frac{dn}{dx} = -sn_\infty\bar{n}(1 - \bar{n}) \tag{17}$$

In Fisher's analysis, it was concluded that for traveling wave solutions to be present, the following inequality must hold true

$$u \geq 2\sqrt{\mathcal{D}s} \tag{18}$$

Applying the derived parametric relationships, the traveling wave profile is plotted in Figure 16. The graph considers two fronts traveling at two arbitrary velocities (.6235m/s and .8235m/s) to show the general shape of the solutions and the interplay of parameters involved.
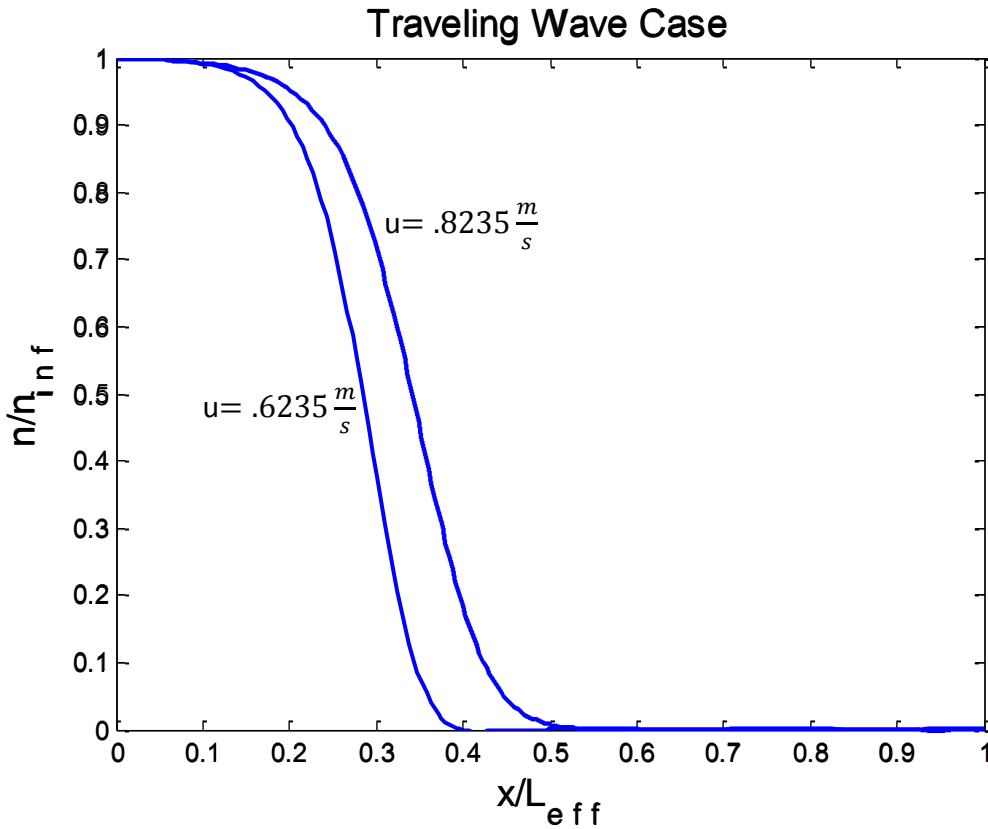
Figure 16: Traveling wave solution, s/D = 2/.08

The traveling wave is an effective way of modeling the cellular fronts as they move over time. In this model, n is assumed to be a continuous variable. However, in reality, in this assay,

cells either occupy a particular location in space or there may be a void. Thus, realistically, cell number density is much more binary, varying between n and 0. The traveling wave approach helps create this contrast by setting up a sharp gradient between the cell region and the no-cell region.

The traveling wave may be set up only for particular values of s and $\mathcal{D}$ as seen in Equation 19. Moreover, as s is increased, the gradient tends to be sharper. Generally to achieve traveling waves with sharp gradients for this particular assay, the value of the nondimensional source term $sn_\infty \bar{n}(1 - \bar{n})$ must share a similar order of magnitude as the value of the expression $\frac{\mathcal{D}}{L_{eff}^2} \frac{d^2\bar{n}}{d\bar{x}^2}$.

Chapter 6

Two-Dimensional Governing Equation for Cell Migration

To this point, spatial variation in only one dimension has been considered. Based on special cases of the one-dimensional governing equation, the modeling parameters have been better understood. In order to model cellular movement in the entire assay, however, it is now necessary to consider cellular movement in both horizontal (x) and vertical (y) dimensions. When the control volume approach presented in Section 5.1 is extended two dimensions, the following two-dimensional governing equation results:

$$\frac{\partial n}{\partial t} = \mathcal{D}_x \frac{\partial^2 n}{\partial x^2} + \mathcal{D}_y \frac{\partial^2 n}{\partial y^2} + sn(n_\infty - n) \tag{19}$$

Note that now diffusion is considered both in the x and y directions. For the sake of convenience, Equation 19 can be written in terms of the flux vector $\vec{\Gamma}$ as follows:

$$\frac{\partial n}{\partial t} + \vec{\nabla} \cdot \vec{\Gamma} = sn(n_\infty - n) \tag{20}$$

$$\text{Where } \vec{\Gamma} = -\mathcal{D}\nabla n \tag{21}$$

6.1) Analysis Using COMSOL

Solving a two-dimensional partial differential equation with a non-linear source term as in Equation 20 can be time-consuming and computationally complex. For the sake of convenience, COMSOL Multiphysics software was used as a platform for solving Equation 20. COMSOL is a software program that uses advanced numerical methods for modeling and simulating physics-based problems. All simulations in this research were created with the MUMPS parallel sparse direct solver [18] using the finite element method.

6.2) Model Setup

Upon initiating a COMSOL file, it is essential to specify the geometry upon which the relevant physics are to be solved. For the case of the assay, a rectangle the size of the initial gap from each experiment was chosen to be the structure. Next, the relevant governing equations

were chosen from the list of available physics icons in the software. Once the relevant governing equation is entered, boundary conditions must be prescribed. This may be done visually as shown in Appendix C. Figure 17 shows an example of the gap geometry with the prescribed boundary conditions. Note that for this specific case, Dirichlet boundary conditions were used at the right and left boundary to set the value of the dependent variable to n_∞. Neumann boundary conditions were used at the top and the bottom to indicate zero-flux in the y-direction initially. A description of the specific steps involved in configuring the simulation file is given in Appendix C.
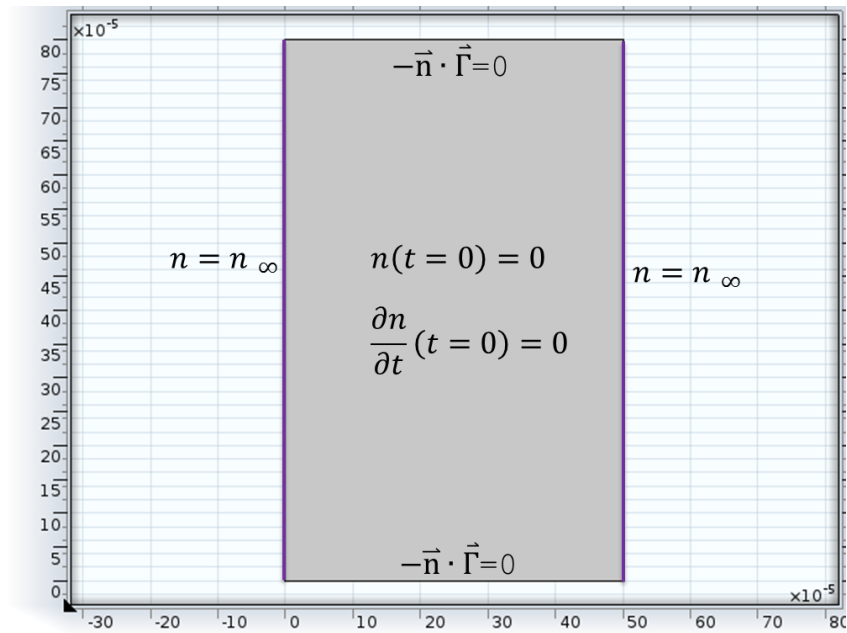
Figure 17: Gap geometry and boundary conditions

6.3) *Generating the Mesh*

In a problem described by Equation 20 where stability is an issue, grid size plays a key role in determining the existence of a solution. For areas in the geometry where gradients are high, the solution only converges if the grid size is small enough. Although having a small grid size means greater accuracy, it also means that there are more elements to solve for, and therefore a significantly greater computational time. Fortunately, COMSOL offers adaptive mesh refinement, whereby, the grid size is made finer in the specific parts of the geometry that demand greater accuracy, whereas the grid size elsewhere remains coarse. The mesh therefore consists of non-uniform elements and is changed and adapted at every time step of the solution. The

26

adaptive mesh feature was utilized for all the simulations in this research. Moreover, for saving additional time, typical time-steps utilized were on the order of 10s to 100s intervals. This approach saved a significant amount of time – the average simulation that could take anywhere between two and five hours to run with a uniform mesh and smaller time-steps was solved in between half-an-hour and an hour.
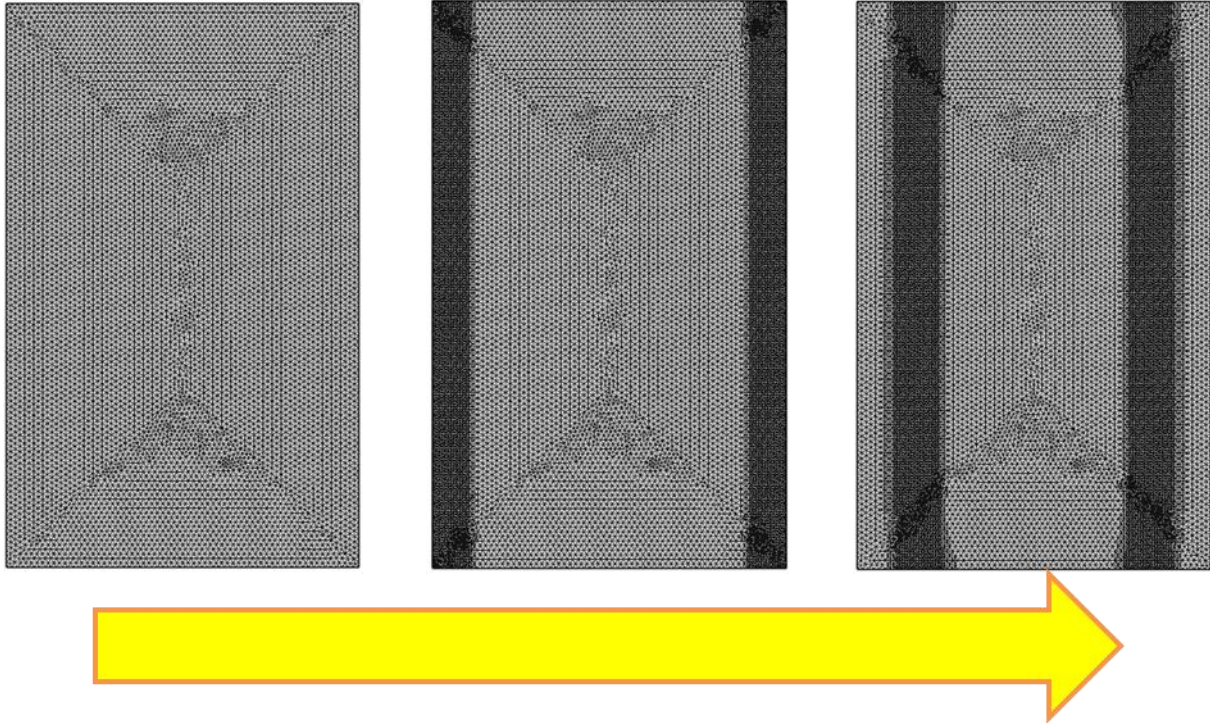
Figure 18: Adaptive mesh refinement

6.4) Effect of Electric Field

In order to account for the change in cellular movement in the presence of an electric field in the model, an analog was drawn to ion mobility theory in gases and liquids. This is considered acceptable as the cells are expected to have a distribution of surface charge and can therefore be treated as massively charged ions. In the presence of an electric field, ions experience some average drift velocity that can be written as:

$$v_{avg} = \mu \vec{E} \tag{22}$$

where μ is the ionic mobility and takes into account particle motion in the presence of collisions with other particles. The same idea is applied here to cellular movement in the presence of an electric field. This mobility theory can be incorporated into the flux vector in Equation 20 as:

$$\vec{\Gamma} = -D\nabla n + \mu \vec{E} n \qquad (23)$$

The value for cellular mobility μ is to be inferred experimentally after determining all other parameters of the model from the relevant control experiments. It must be noted that for the sake of simplifying the equation, a constant value of $\vec{E}$ is assumed for the models in this work. In the experiments, the value of the electric field actually varied with time. Therefore, the constant value assumed for $\vec{E}$ was taken to be a representative average value of $\vec{E}(t)$ over the duration of the experiment.

6.5) *Inferring Parameters*

Appropriate values for the parameters $D_x, D_y, s,$ and n_∞ can be obtained from the model if the model predictions are matched to the experimental observations in the control cases. These parameters are specific to the specific experimental situation, which takes into account the type of cells being used, the cell culture, and other environmental variables. Next, an appropriate value for μ can be inferred if the model predictions are matched to the experimental observations when the electric field is applied.

Whereas in reality, the magnitude and direction of the electric field changed over time in the experiments, a constant value 4.4mV/cm is assumed for the electric field in the horizontal (x) direction in the simulation.

In order to make the model match the experimental results, reasonable initial estimates of $D_x, D_y, s,$ and n_∞ need to be made to initiate the fine-tuning process of matching model to experiment. It is appropriate to begin with finding a value for u, since a constant-velocity traveling wave approach is used for finding the solutions in the model as described in Section 5.3.3. u can be estimated from the experimental results by monitoring the distance a cell front has traveled over the course of the experiment and dividing that by the duration of the experiment:

$$u = \frac{\Delta L}{\Delta \tau} \qquad (24)$$

As can be seen in Figure 7, it is reasonable to assume that u is indeed constant.

Next, D can be estimated in a similar manner dimensionally as:

$$\mathcal{D}_x \sim \frac{(\Delta L)^2}{\Delta \tau} \qquad (25)$$

Since u and $\mathcal{D}_x$ are now known, s can be estimated through the traveling wave parametric condition described in Equation 18. Rearranging Equation 18, a maximum value for s can be found:

$$s \leq \frac{u^2}{4\mathcal{D}_x} \qquad (26)$$

Finally, since n_∞ is defined as the cell number density away from the gap, it can be calculated by estimating confluency in the cell culture as:

$$n_\infty = \frac{Number\ of\ cells}{Volume} \qquad (27)$$

Appendix B shows the sample calculations used to arrive at the initial estimates for both experiments that are modeled in this thesis.

Chapter 7

Results

7.1) Overview

Upon estimating initial values for the parameters as described in Section 6.5, the governing equation (Equation 20) was solved using COMSOL Multiphysics. At every 4-hour time increments of simulated time (which corresponded to approximately eight to ten minutes of computer run time), the model was compared to the experiment for gap closure.

In order to calculate the gap closure percentage in the model, a criterion for differentiation between cell and gap had to be developed within the traveling wave. It was decided that the inflection point of the traveling wave would be taken as the interface between cell and gap. In order to find the inflection point of the two converging waves, COMSOL was used to obtain the one-dimensional profile plots of n. MATLAB was used to find the appropriate inflection points and subsequent cell-gap thresholds through numerical differentiation. The MATLAB script used to find the inflection points of the traveling waves is provided in Appendix D.

Once the area of the gap was found, the percent closure was calculated and compared to the experimental counterpart. If the values were not within ±5% of each other, the parameters were fine-tuned appropriately, and the simulation was repeated with the new values of the parameters.

The parameters $\mathcal{D}_x, \mathcal{D}_y, s,$ and n_∞ that were acquired from the control experiments were used again in the simulations with the electric field. It was anticipated that the mobility can be varied until the gap closure observed in the experiments was replicated in the simulations for the case of the applied electric field.

7.2) Gap Closure in the Control Case

In the experimental control case for Keratinocytes in the scratch assay, the gap closure after 4 hours was 25.11% and the gap closure after 8 hours was 53.71% as can be seen in Figure 7. Gap closure here refers to the percentage of the original gap area that is filled in after the

experiment begins. After the values of $D, s, and\ n_\infty$ were found (Table 2), the results shown in Figure 19 and Figure 20 were obtained
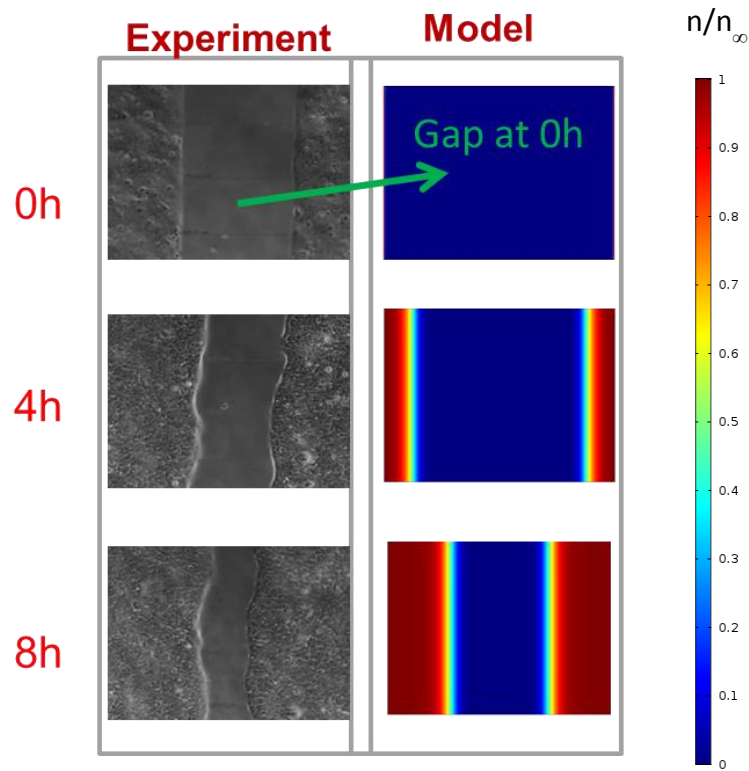

Figure 19: Modeling keratinocyte closure

Figure 20 shows how close the experimental gap closure values were to the modeled ones.
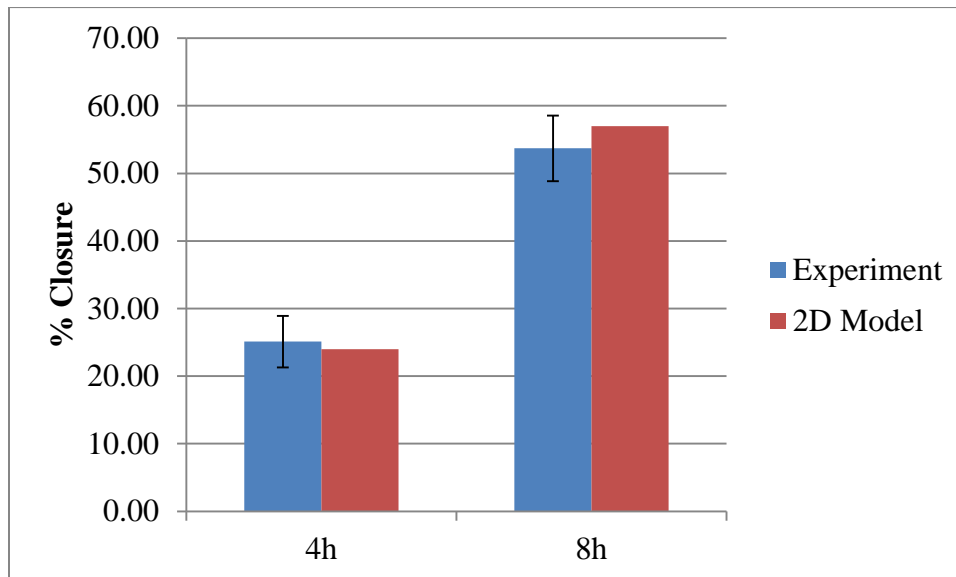
Figure 20: Predicting gap closure - keratinocytes

Table 2 lists the parameters used for this particular model.

Table 2: Model parameters for keratinocytes assay

$\mathcal{D}_x$	$\mathcal{D}_y$	s	n_∞
1.6×10^{-14} m^2/s	1.2×10^{-16} m^2/s	4.2×10^{-19} m^3/s	1.3×10^{15} $cells/m^3$

Despite the close approximation that the model delivers, it fails to capture such artifacts as the wavy cell fronts in the experiment. This suggests that the model needs to be refined in order to capture certain nuances of experiment.

In the experimental control case for SCP2 cells in the scratch assay, the gap closure after 16 hours was 43% as can be seen in Figure 9. The model was fit to behave like the experiment, and Figure 21 below shows the results compared to the corresponding images from the experiment.

Figure 21: Modeling SCP2 cell closure

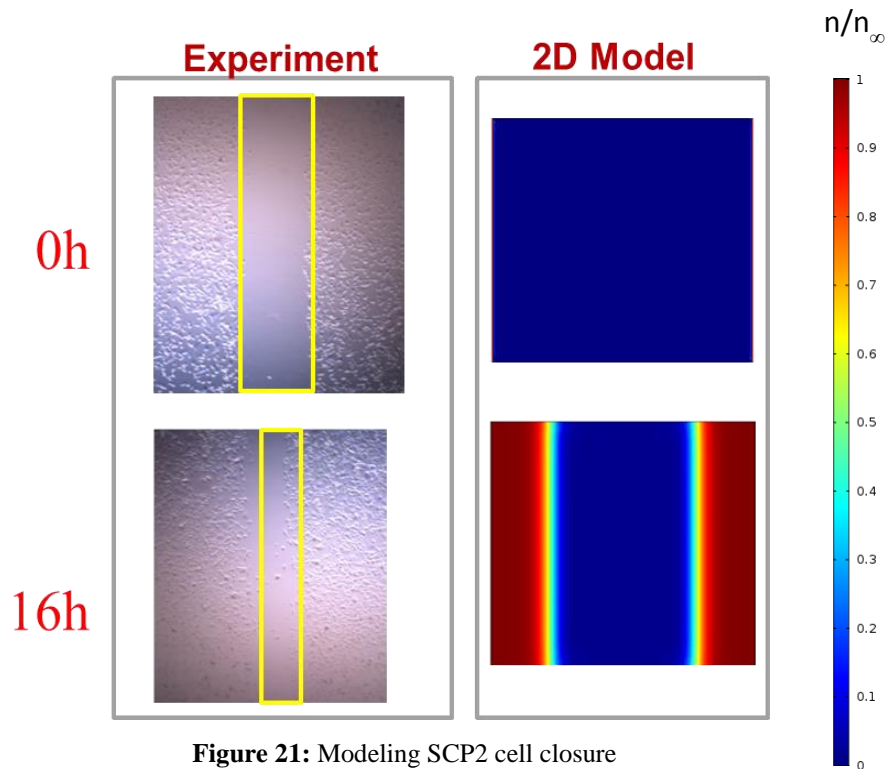Figure 22 shows how close the experimental gap closure values were to the modeled ones.
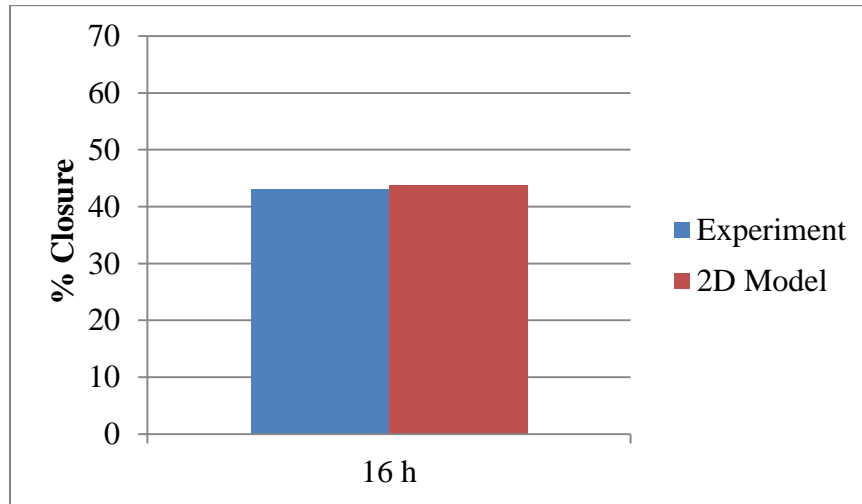
Figure 22: Predicting gap closure - SCP2 cells

Table 3 lists the parameters used for this particular model.

Table 3: Model parameters for SCP2 assay

D_x	D_y	s	n_∞
3.2×10^{-14} m^2/s	0 m^2/s	2.25×10^{-19} m^3/s	1×10^{15} $cells/m^3$

Note that since there was not enough contrast in the experimental image to determine motion in the y-direction, a diffusivity of 0 was assumed in that direction.

It must also be noted that the order of magnitude for the diffusivity values acquired through both of the above simulations were about the same as presented in a model for cell migration by Vanegas-Acosta et al. that considered cell movement of osteoblasts in a different assay geometry [15].

7.3) Predicting Gap Closure – Electric Field Case

Using the parametric values inferred in the control case, an electric field of 4.4mV/cm in the horizontal (x) direction was introduced in the model, and the mobility was gradually increased.

For low values of mobility ($\mu<10^{-8}m^2$/Vs), the gap closure remained the same as the control case. Here, the electric field expression failed to make a significant contribution to the flux term in Equation 20.
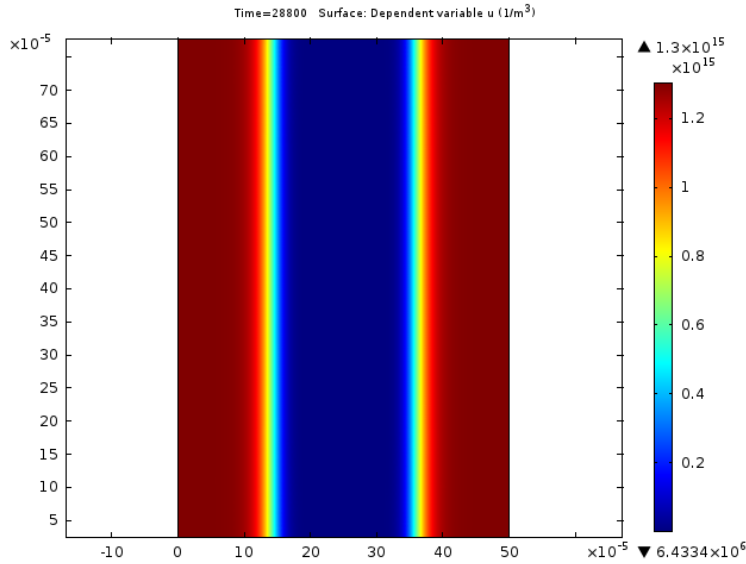
Figure 23: Asymmetric closure. $\mu= 8x10^{-9}m^2$/Vs. Gap Closure: 54%

As mobility was increased to $\mu=5x10^{-7}m^2$/Vs, asymmetric closure was observed in the simulations. One cell front advanced faster (in this case the left one), while the other one advanced slower than the control case. However the gap closure at the end of the simulated 4 hours (which was approximately half an hour of computer run time) remained about the same as the control case. An inhibition of closure was not observed.
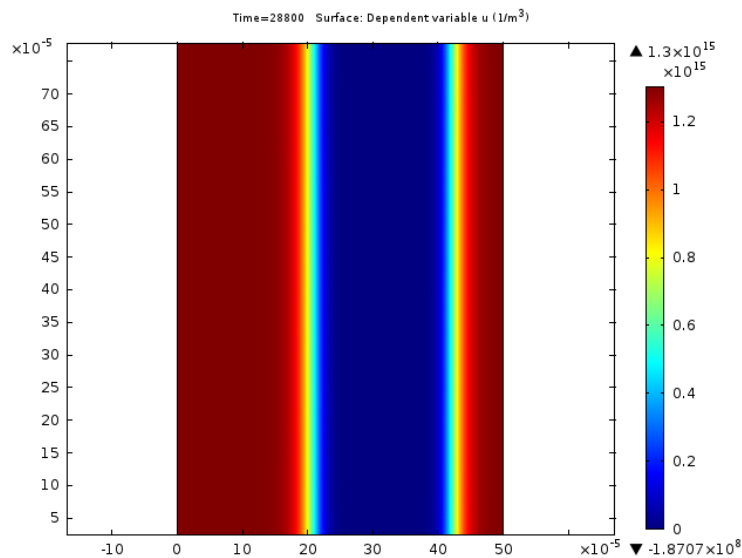
Figure 24: Asymmetric closure. $\mu= 5x10^{-7}m^2$/Vs. Gap Closure: 54%

As mobility was further increased to $2x10^{-6}m^2$/Vs, the rightmost cell front failed to advance at all, while the leftmost cell front (Figure 25) advanced even faster than before. Here, at the end of the simulated 4 hours, gap closure actually increased. This obviously does not correspond to the behavior of the cells observed experimentally.

Time=28800   Surface: Dependent variable u ($1/m^3$)

Figure 25: Asymmetric closure. μ= $2x10^{-6}m^2$/Vs. Gap Closure: 76%

The simulation was rerun, this time changing the direction of the applied electric field. The very same trends of *accelerated closure* were apparent, but this time the asymmetry was in the opposite direction as Figures 24 and 25. This is illustrated in Figure 26.
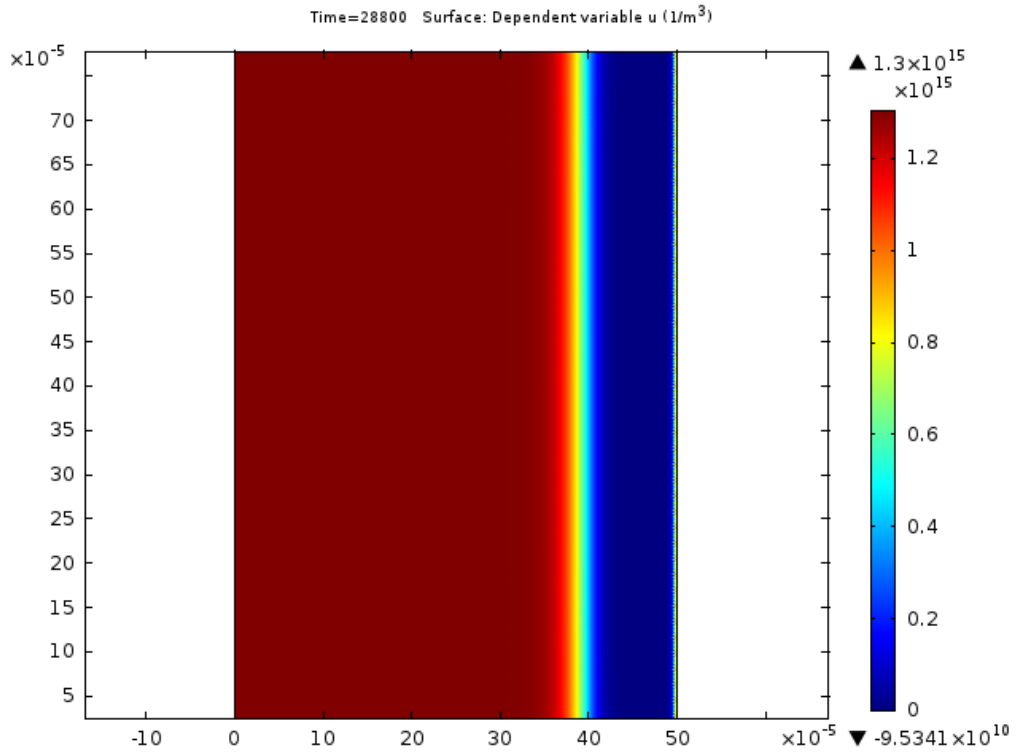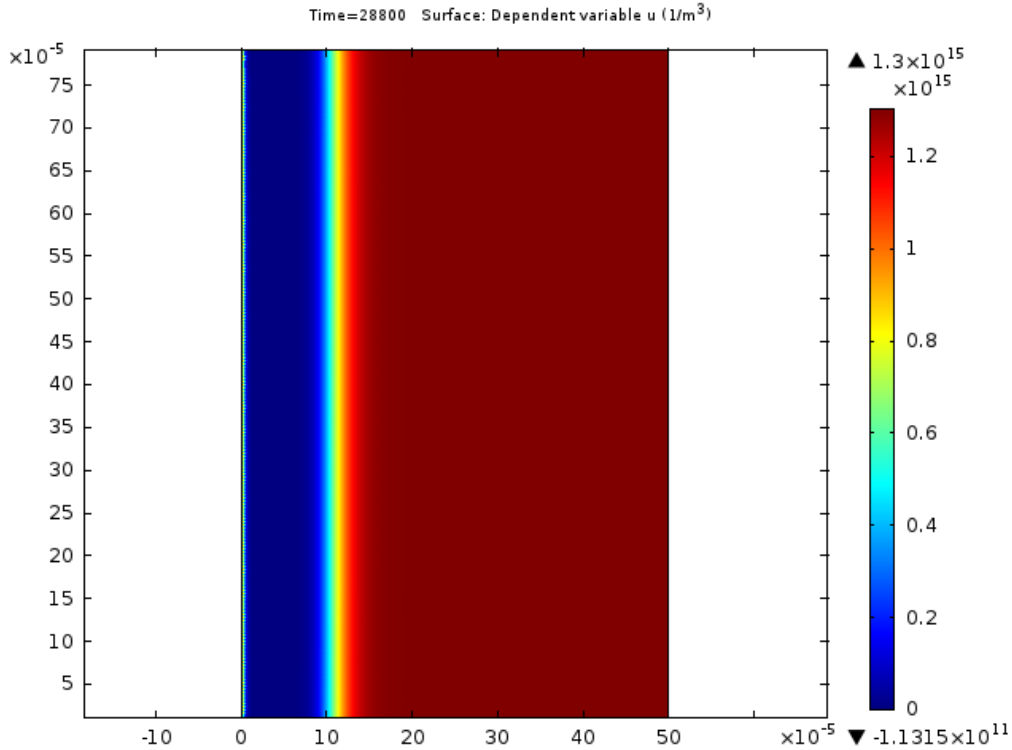
Figure 26: Asymmetric closure. $\mu = 2 \times 10^{-6} \text{m}^2/\text{Vs}$. Gap Closure: 76%

Similar behavior was noticed for the SCP2 cell model. Appendix A contains the images and data from varying mobility in the SCP2 model.

When incorporating the electric field, the ion mobility theory analog that was assumed in Section 6.4 along with a constant value for $\vec{E}$ was only able to lead to *accelerated* closure, but never *inhibited* closure. It is possible to model inhibition of closure, but to do so, it is necessary to change the value of diffusivity as can be seen in Figure 31 in Appendix A. However, diffusivity is assumed to be a property of the cells and cell culture as it is inferred from the control experiments, and hence it must remain the same even when the electric field is present. The fact that it must also change in order to explain the experimental results suggests that the presence of the electric field has altered some fundamental property of the cells that they possess even in the absence of the field.

A constant value was assumed for the electric field in the model which did not reflect the time-varying electric field present in the experiments. Therefore, future refinements of the model would have to account for a time-varying electric field. However, since the electric field varies

over time on the order of tens of nanoseconds, and the time-steps incorporated in the simulations were on the order of tens of seconds, an appropriate non-dimensional scheme must be developed to be able to solve Equation 23 with a time-varying electric field input in a reasonable amount of computer run time. Moreover, the time-varying input may also introduce instabilities that must be addressed by appropriately setting up the solver. Hence, more work needs to be done to refine the model that takes into account a time varying electric field input.

Summary and Conclusions

This thesis has explored the use of the non-linear reaction-diffusion equation to simulate scratch assay cell migration experiments, with and without the presence of an induced electric field. A better understanding of electrotaxis offers the promise of finding ways to artificially accelerate (as in wound-healing) or decelerate (as in cancer metastasis) cells as desired. Conventional methods of studying electrotaxis involve the use of agar bridges to directly contact the cell culture to the metal electrode in order to apply an electric field. Such an approach can introduce electrochemical contaminants and undesirable Ohmic heating effects.

The focus of this research was to analyze experiments conducted on cells through a non-contact application of an electric field and then to develop an appropriate model to quantify and eventually predict experimental results. Non-contact here is achieved inductively through a time-varying current driven through a coil. Experiments were conducted in a "wound healing assay" for keratinocyte cells and highly metastatic breast cancer (SCP2) cells, and it was noted that upon the application of an electric field, the movement of the cell fronts was inhibited significantly in both cases.

By assuming that the cells form a monolayer and that cellular number density can be characterized as a continuous variable, a model was developed that utilized a control volume approach to derive a two-dimensional governing partial differential equation. The Fisher-Kolmogorov Equation is a one-dimensional special case of this equation and is solved by R.A. Fisher [13] to provide the parametric relationships that generate constant-velocity traveling wave fronts. The traveling wave approach was used to track the movement of the closing cell fronts in time and space. In order to account for cell movement in the presence of an electric field, ion mobility theory was used as an analog and appended to the model.

COMSOL Multiphysics finite element software was used in conjunction with an adaptive meshing feature to generate the two-dimensional simulations of the governing differential equation. By matching model to experiment in the control case, the relevant parameters from the model were inferred. Inferred diffusivity values were on the same order of magnitude as diffusivities presented in a cell migration model for osteoblasts by Vanegas-Acosta [15].

When the electric field cases were simulated, closure was noticed to be asymmetrical. Upon varying the value of cellular mobility, the net closure either remained the same or increased as a result of higher mobility values. One possible reason for the ion mobility model

38

not conforming to experimental results is that the electric field may in fact be affecting some fundamental cellular mechanism, thereby changing the value of cell diffusivity from the control case. It may also be noted that while a constant value of the electric field was assumed in the model, in reality, the electric field applied periodically changed magnitude and direction. The model therefore must be refined to take into account time-varying electric fields.

Despite its shortcomings, a viable model was developed that allows for quantification of migration assays. This may serve as a useful tool for biologists and researchers to ensure that control cases are indeed similar. Further development of this model may also shed more light into the phenomenon of electrotaxis.

Recommendation for Future Work

The model developed in this research may be improved in several aspects. First, it is instructive to run more simulated cases of the governing equation to see the different patterns and profiles that are possible. Some of these cases may be computationally expensive, and it may be useful to run some cases through a supercomputer to see if certain nuances or artifacts of experimental cell motion can be modeled. Second, more work needs to be done into understanding the electric field model and whether it is possible to computationally inhibit closure with an electric field present. One way to do this is to enter a realistic time varying electric field (in pulses). However, such an approach may be computationally demanding. Finally, the validity of the model should be examined for different electric field strengths, frequencies, cell types, and other assay geometries. Once a robust model is created, it would be possible to optimize subsequent experiments and experimental outcomes using the predictions from the model.

Appendix A: Figures and Tables
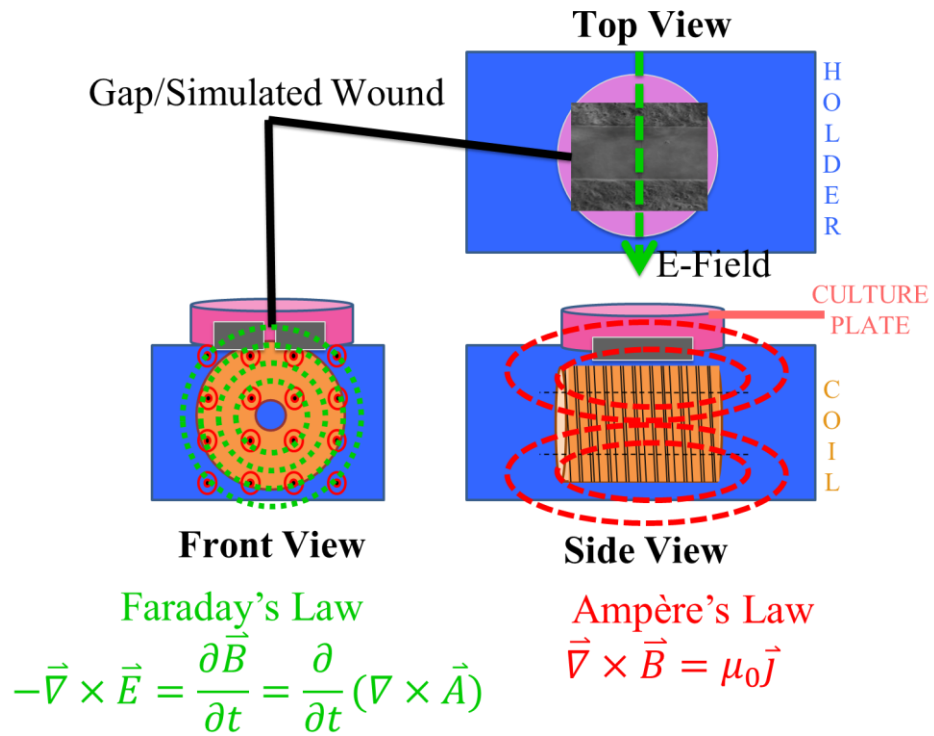
Figure 27: Electromagnetic principles underlying non-contact application of electric field
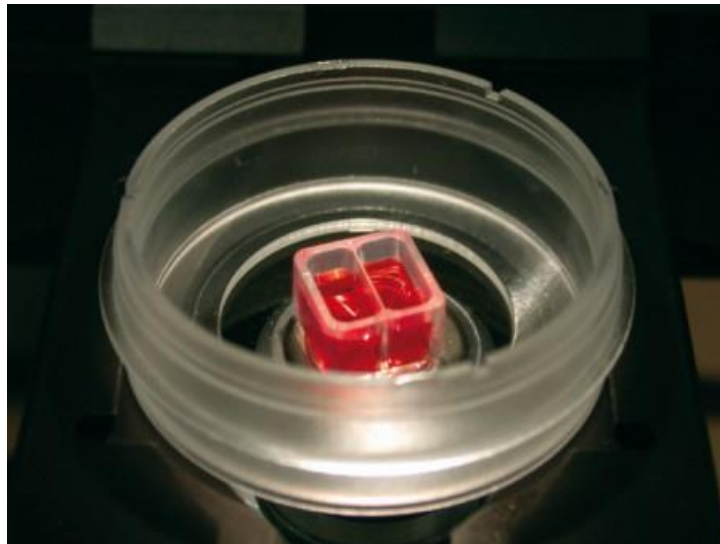
Figure 28: Cell culture insert. Source: http://ibidi.com
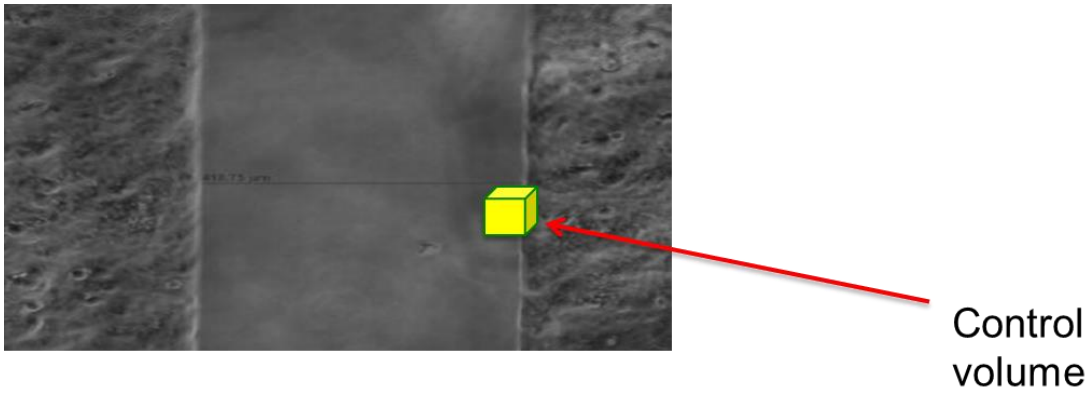
Figure 29: Control volume inside the assay geometry

$\mu= 8\times10^{-9}m^2/Vs$
Gap Closure: 44%
Same as control

$\mu= 2\times10^{-7}m^2/Vs$
Gap Closure: 44%
Same as control

$\mu= 1.2\times10^{-6}m^2/Vs$
Gap Closure: 51%
Greater than control
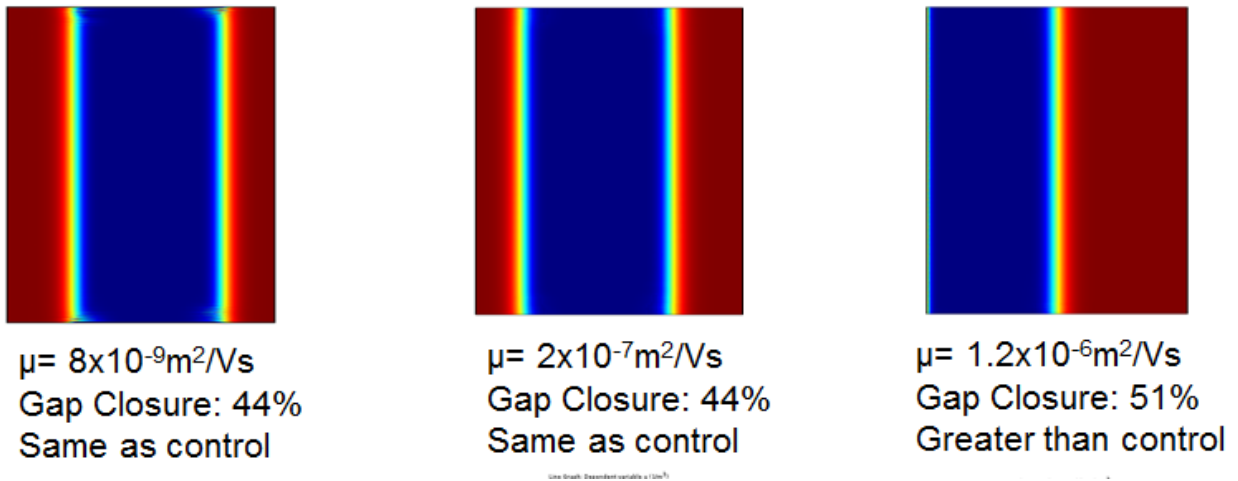
Figure 30: Acceleration with constant electric field model - SCP2 cells
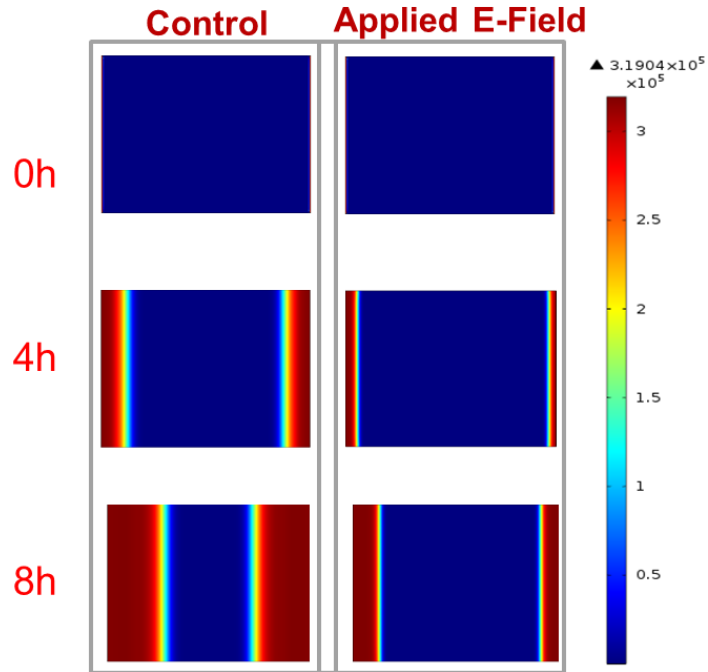
Figure 31: Changing diffusivity in the applied electric field case to account for inhibited closure

Table 4: Parameters that correspond to the control and electric field case in Figure 30

$\mathcal{D}_x$	$\mathcal{D}_{x,EF}$	$\mathcal{D}_y$	s	n_∞	E_x	E_y	μ
1.6×10^{-14} m^2/s	2.5×10^{-15} m^2/s	1.2×10^{-16} m^2/s	4.2×10^{-19} m^3/s	1.3×10^{15} $cells/m^3$	$.044$ V/m	0 V/m	5×10^{-9} m^2/Vs

Appendix B: Sample Calculations

I. Analytical Solution for Spatially Homogeneous Special Case

$$\frac{d\bar{n}}{dt} = sn_\infty \bar{n}(1 - \bar{n})$$

Let some $w = \bar{n}^{-1}$

$$w' = -\bar{n}^{-2} \cdot \bar{n}'$$

$$-w' = \bar{n}^{-2} \cdot sn_\infty \bar{n}(1 - \bar{n})$$

$$-w' = sn_\infty \bar{n}^{-1}(1 - \bar{n})$$

$$w' + sn_\infty w = sn_\infty$$

$$w = 1 + Ce^{-sn_\infty t}$$

Thus,

$$\bar{n} = \frac{1}{1 + Ce^{-sn_\infty t}}$$

Assuming an initial condition where $\bar{n}(0) = \frac{n_i}{n_\infty}$

$$\frac{n_i}{n_\infty} = \frac{1}{1 + C}$$

$$C = \frac{n_\infty}{n_i} - 1$$

Therefore,

$$\bar{n} = \frac{1}{1 + \left(\frac{n_\infty}{n_i} - 1\right)e^{-sn_\infty t}}$$

45

II. Initial Parameter Estimation for Keratinocyte Model

$$u = \frac{\Delta L}{\Delta \tau} \approx \frac{250 \mu m}{8hr} = 8.68 \times 10^{-9} \frac{m}{s}$$

$$\mathcal{D} \sim \frac{(\Delta L)^2}{\Delta \tau} \approx \frac{(250 \mu m)^2}{8hr} = 2.17 \times 10^{-12} \frac{m^2}{s}$$

The above value of $\mathcal{D}$ can be compared to the inferred value in the model of $\mathcal{D}_x = 1.6 \times 10^{-14} \frac{m^2}{s}$

$$s \leq \frac{u^2}{4\mathcal{D}} \rightarrow s \leq \frac{(8.68 \times 10^{-9})^2}{4 \times 2.17 \times 10^{-12}} = 8.7 \times 10^{-6}$$

The above range of s can be compared to the inferred value in the model of $s = 4.2 \times 10^{-19} \frac{m^3}{s}$

$$n_{\infty} = \frac{\# \, of \, cells}{Volume}$$

Assuming the radius of the culture dish is about 2.5cm, the radius of a keratinocyte cell is about 10µm, and the thickness of a cell is about 10µm:

$$\# \, of \, cells = \frac{A_{culture \, dish}}{A_{cell}} = \frac{\pi R^2_{culture \, dish}}{\pi R^2_{cell}} = \frac{\pi (.025)^2}{\pi (10 \times 10^{-6})^2} = 2.5 \times 10^7 cells$$

$$Volume = A_{culture \, dish} \times t_{cell} = \pi(.025)^2 \times 10 \times 10^{-6} = 2 \times 10^{-8} m^3$$

$$n_{\infty} = \frac{2.5 \times 10^7 cells}{2 \times 10^{-8} m^3} = 1.3 \times 10^{15} \frac{cells}{m^3}$$

II. Initial Parameter Estimation for SCP2 Model

$$u = \frac{\Delta L}{\Delta \tau} \approx \frac{473 \mu m}{16hr} = 8.22 \times 10^{-9} \frac{m}{s}$$

$$\mathcal{D} \sim \frac{(\Delta L)^2}{\Delta \tau} \approx \frac{(473 \mu m)^2}{16hr} = 3.88 \times 10^{-12} \frac{m^2}{s}$$

The above value of $\mathcal{D}$ can be compared to the inferred value in the model of $\mathcal{D}_x = 3.2 \times 10^{-14} \frac{m^2}{s}$

$$s \leq \frac{u^2}{4\mathcal{D}} \rightarrow s \leq \frac{(8.22 \times 10^{-9})^2}{4 \times 3.88 \times 10^{-12}} = 4.4 \times 10^{-6}$$

The above value of s can be compared to the inferred value in the model of $s = 2.25 \times 10^{-19} \frac{m^3}{s}$

$$n_\infty = \frac{\# \; of \; cells}{Volume}$$

Assuming the radius of the culture dish is about 2.5cm, the radius of a keratinocyte cell is about 10μm, and the thickness of a cell is about 10μm:

$$\# \; of \; cells = \frac{A_{culture \; dish}}{A_{cell}} = \frac{\pi R_{culture \; dish}^2}{\pi R_{cell}^2} = \frac{\pi (.025)^2}{\pi (10 \times 10^{-6})^2}$$

$$= 2.5 \times 10^7 cells \; \times .8 \; confluency = 2 \times 10^7 cells$$

$$Volume = A_{culture \; dish} \times t_{cell} = \pi (.025)^2 \times 10 \times 10^{-6} = 2 \times 10^{-8} m^3$$

$$n_\infty = \frac{2 \times 10^7 cells}{2 \times 10^{-8} m^3} = 1 \times 10^{15} \frac{cells}{m^3}$$

Appendix C: Explanation of the Software

Explanation of COMSOL Multiphysics

COMSOL Multiphysics' user interface is visually driven and relatively easy to use. This Appendix describes the steps involved in creating and analyzing a model in COMSOL.

Upon opening a new file in COMSOL, one is prompted to select the type of physics that is to be solved. The format that most closely matches the model developed in this paper is called "**General Form PDE**" under the Mathematics tab (Figure 32).
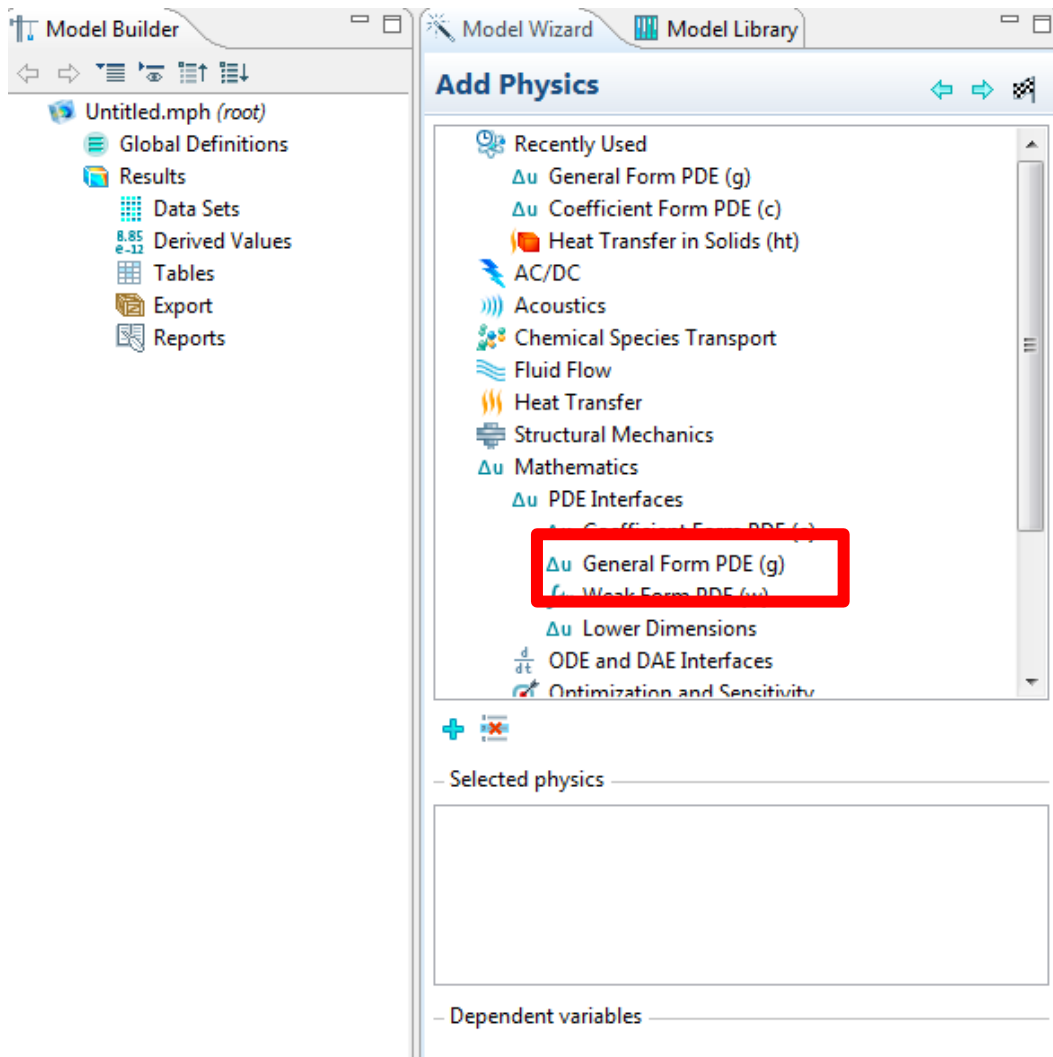

Figure 32: Initiating a model in COMSOL

The next task in setting up the model is defining the geometry onto which the relevant equations need to be solved. Right clicking **Geometry** on the **Model Builder** pane reveals a list of possible 1-D and 2-D figures available (Figure 33). For this model, **Rectangle** is selected and appropriate

49

dimensions are ascribed to model the gap in the wound-healing assay (Figure 16).
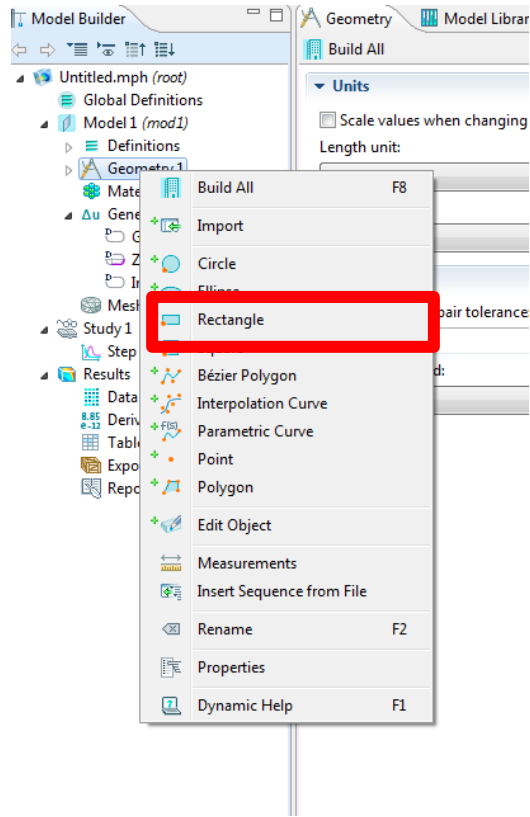
Figure 33: Geometry selection in COMSOL

Next, the essential parameters can be entered by selecting **Parameters** under **Global Definitions** in the **Model Builder** pane. Once parameter values are entered, units can be entered explicitly using brackets as shown in Figure 34.

Figure 34: Entering parameters with units in COMSOL

Next, selecting **Model >> General Form PDE** opens up the pane to enter the governing equation or equations. COMSOL actively checks units, and raises an error if units are mismatched as the equation is entered.

Figure 35: Entering the governing equation in COMSOL

When selecting a mesh, it is most practical to check off **Adaptive Mesh Refinement** under **Study >> Step 1: Time Dependent.** The simulation can then be run by right clicking **Study** and then clicking **Compute**.

Next comes the task of prescribing boundary conditions. Right clicking on **General Form PDE** shows a list of boundary conditions that can be used for the simulation. Upon selecting a desired boundary condition, the value or expression may be entered and ascribed to a boundary visually. For the simulations in this paper, the Dirichlet Boundary Condition and the Zero Flux condition were most heavily utilized.
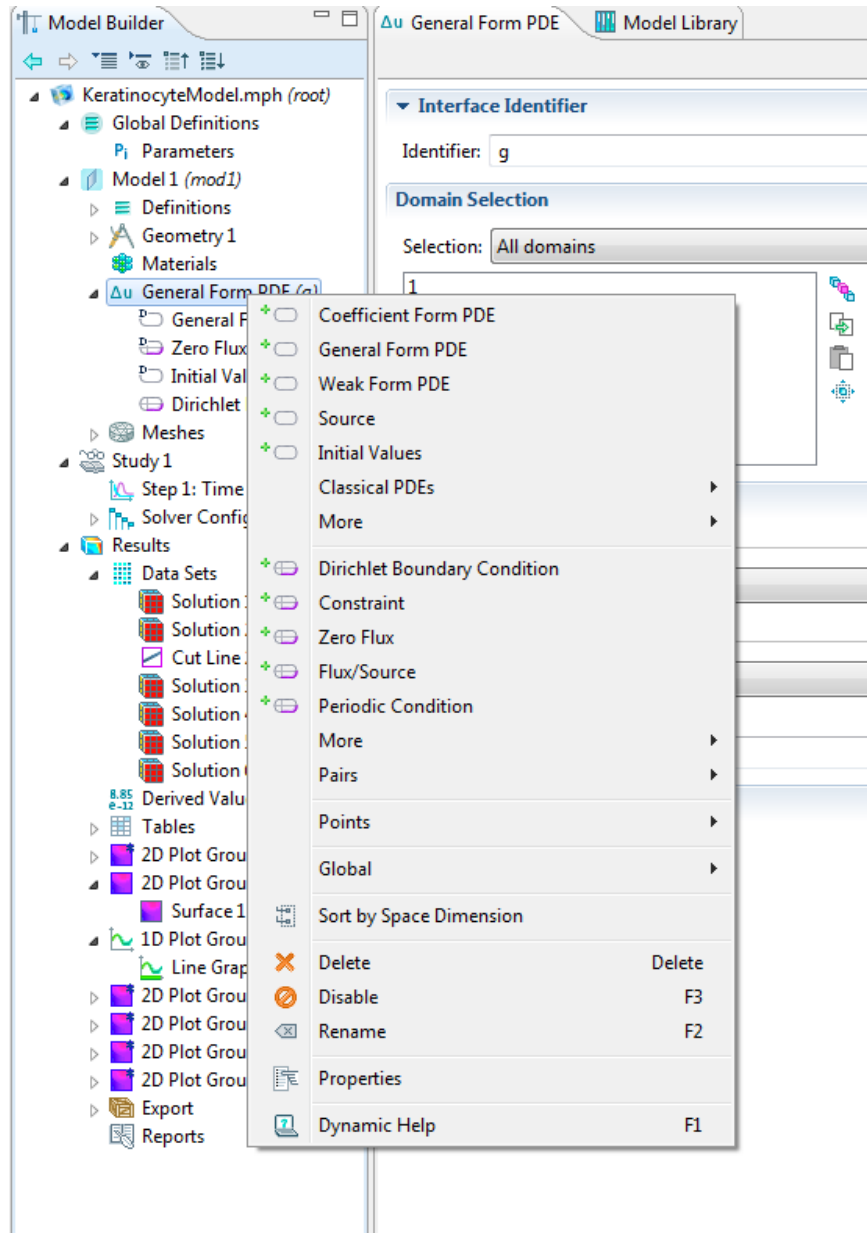
Figure 36: Possible boundary conditions in COMSOL

Once the simulation is run, results are generated and displayed under **2D Plot Group**. To generate a1-D profile view, a **Cut Line 2D** must be created in the geometry. This may be done by right clicking on **Data Sets**. Next, a **1D Plot Group** must be created by right clicking on **Results** to graph the values of the dependent variable along the line created in **Cut Line 2D** versus some other variable.

All of the data can be conveniently exported as a spreadsheet by right clicking the appropriate dataset and clicking on **Add Plot Data to Export**. Movies of the simulation can be conveniently created in the same manner.
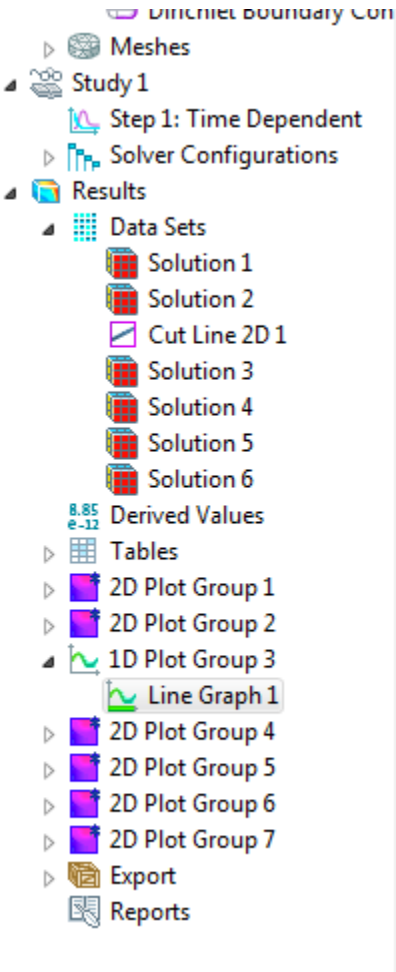
Figure 37: Data analysis features in COMSOL

Appendix D: MATLAB Scripts

SpatiallyHomogeneous_nbar.m

```
%Anu Kaushik
%Reduction-Diffusion Equations

%This program numerically solves for cell density in the
spatially
%homogeneous special case for the governing one-dimensional PDE.
The result
%is plotted in Figure 11

%The Ohio State University
%Department of Mechanical and Aerospace Engineering


[t,n_bar] = ode45(@changen_nbar,[0,600],.001);

plot(t,n_bar,'LineWidth',2);
xlabel ('Time (s)','FontSize',14)
ylabel ('n/n_i _n _f','FontSize',14)
title('Spatially Homogenous Case','FontSize',14)
```

changen_nbar.m

```
function [ dn ] = changen_nbar( t,n_bar )

%   This function file is the input to SpatiallyHomogeneous_nbar
and
%   describes the parameters used in the plot in Figure 11

s=.000000001;
n_inf = 2.5e7;

dn = s*n_inf*n_bar*(1-n_bar);
end
```

SpatiallyHomogeneous_nbar.m

```
%Anu Kaushik
%Reduction-Diffusion Equations

%This program numerically solves for cell density in the steady
state
%special case for the governing one-dimensional PDE. The results
%are plotted in Figure 12 and 14

%The Ohio State University
%Department of Mechanical and Aerospace Engineering

[x_bar,n_bar] = ode45(@sschange_nbar,[0,1],[.01,0]);

plot(x_bar,n_bar(:,1),'LineWidth',2);
xlabel ('x/L _r _e _f','FontSize',14)
ylabel ('n/n_i _n _f','FontSize',14)
title ('Steady State Case','FontSize',14)
```

sschangen_nbar.m

```
function [ dn ] = sschange_nbar( x,n_bar )

%   This function file is the input to SteadyState_nbar and
%   describes the parameters used to plot Figures 12 and 14
s=3; %3e-2
D=1; %1e2
n_inf = 1;
Lref = 1;

dn = [n_bar(2)
      -1*Lref^2/D*s*n_inf*n_bar(1)*(1-n_bar(1))];



end
```

TravelingWave_nbar.m

```matlab
%Anu Kaushik
%Reduction-Diffusion Equations

%This program numerically solves for cell density in the
constant velocity
%traveling wave special case for the governing one-dimensional
PDE. The result
%is plotted in Figure

%The Ohio State University
%Department of Mechanical and Aerospace Engineering
clc; clear all;



[x_bar,n_bar] = ode45(@travwave_nbar,[0,1],[.999,0]);


plot(x_bar,n_bar(:,1),'LineWidth',2);
axis([0,1,0,1]);


xlabel ('x/L_e _f _f','FontSize',14);
ylabel ('n/n_i _n _f','FontSize',14);
title ('Traveling Wave Case','FontSize',14);
```

travwave_nbar.m

```matlab
function [ dn ] = travwave_nbar( x_bar,n_bar )

%   This function file is the input to TravelingWave_nbar and
%   describes the parameters used to plot Figures 15

  Lref = 10; n_inf = 1.0001;  D =.08; s= 2; uref = .82325;
  u_bar = 1;

dn = [n_bar(2)
    -1*Lref*uref*u_bar/D*n_bar(2) + -
1*Lref^2/D*s*n_inf*n_bar(1)*(1 - n_bar(1))];



end
```

inflectionpoints.m

```matlab
%Anu Kaushik

clear all;
clc;
%This program finds the area of the gap in the wound-healing
assay computational model
%by finding the points of inflection of the traveling wave. The
inflection
%points of the traveling wave mark the threshold between cell
and gap in the model

%In a future iteration of this code, as the model starts
developing wavy
%fronts, the entire 2D model would have to be imported and the
inflection points
%have to be found at incremental distances from the bottom of
the geometry
%to the top, as numerical integration is performed.

%The Ohio State University
%Department of Mechanical and Aerospace Engineering

gapwidth = 1100e-6; %in meters, experimentally dependent

data = load('Elec_ker.txt');
d1=diff(data);
d2= diff(d1);
plot(d2(:,2))
l = length(d2);
counter=1;
for i=2:l
    if d2(i-1,2)*d2(i,2)<0 && (d1(i,2)<-3000 || d1(i,2)>3000)
%The value of the first derivative is used to eliminate noise
        xval(counter)=data(i,1);
        counter=counter+1;
    end
end

percentClosure = 1-(xval(2)-xval(1))/gapwidth;
```

References

[1]   C. D. McCaig, A. M. Rajnisek, B. Song, and M. Zhao, "Controlling Cell Behavior Electrically: Current Views and Future Potential", *Physiol. Rev*. 85, pp. 943-978, 2005.

[2]   Subramaniam, V. "Samsung Group Presentation." The Ohio State University, Columbus, OH. 11 Oct. 2012.

[3]   Foulds IS, Barker AT. "Human skin battery potentials and their possible role in wound healing", *British J of Dermatology* 1983; 109:515-522.

[4]   Nishimura KY, IR, Nuccitelli R. "Human keratinocytes migrate to the negative pole in direct current electric fields comparable to those measured in mammalian wounds." *Journal of Cell Science* 1996; 109:199-207.

[5]   Pullar CE, Isseroff RR, Nuccitelli R. "Cyclic AMP-dependent protein kinase A plays a role in the directed migration of human keratinocytes in a DC electric field." *Cell Motility and the Cytoskeleton* 2001; 50: 207-217.

[6]   Zhao M, Pu J, Forrester JV, McCaig CD. "Membrane Lipids, EGF receptors and intracellular signals co-localize and are polarized in epithelial cells moving directionally in a physiological electric field*." FASEB J* 2002; 16(8):857-859

[7]   Chu CS, McManus AT, Pruitt BA, Mason AD. "Therapeutic effects of silver nylon dressings with weak direct current on Pseudomonas aeruginosa-infected burn wounds." *Journal of Trauma Injury, Infection, and Care* 1988; 28: 1488-92.

[8]   "Procellera Technology." <u>Technology</u>. 02 Apr. 2014
<http://procellera.com/procellera/technology>.

[9]   J. Banerjee, P. D. Ghatak, S. Roy, S. Khanna, E. K. Sequin, K. Bellman, B. C. Dickinson, P. Suri, V. V. Subramaniam, C. J. Chang, and C. K. Sen, "Improvement of Human Keratinocyte Migration by a Redox Active Bioelectric Dressing", *PLOS One*, Vol. 9, No. 3, p. e89239, March 2014

[10]   Huo, R., Ma, Q., Wu, J. J., Chin-Nuke, K., Jing, Y., Chen, J., . . . Li, J. (2010). "Noninvasive Electromagnetic Fields on Keratinocyte Growth and Migration." *Journal of Surgical Research.* doi:10.1016/j.jss.2009.02.016

[11]   E. K. Sequin, J. D. West, and V. V. Subramaniam, "Motility of Cells in the Presence of Eddy Currents", Paper NEMB2013-93415 presented at the ASME 2nd Global Congress on Nanoengineering for Medicine & Biology, Boston, Massachusetts, February 4-6, 2013.

[12]   A. Kostic, C.D. Lynch, M.P. Sheetz. "Differential matrix rigidity response in breast cancer cell lines correlates with the tissue tropism." *PLoS ONE*, Vol. 4, p. e6361. 2009

[13]   R. A. Fisher, "The Wave of Advance of Advantageous Genes", *Annals of Eugenics (now Annals of Human Genetics)* Vol. 7, Issue 4, pp. 355-369, 1937.

[14]   Volpert, V., S. Petrovskii. "Reaction–diffusion waves in biology." *Physics of Life Reviews* 6 (2009): 267-310.

[15]   Vanegas-Acosta, J.c., D.a. Garzón-Alvarado, and A.p.m. Zwamborn. "Mathematical model of electrotaxis in osteoblastic cells." *Bioelectrochemistry* 88 (2012): 134-43.

[16]   "Logistic Equation." <u>-- from Wolfram MathWorld</u>. 02 Apr. 2014
<http://mathworld.wolfram.com/LogisticEquation.html>.

[17]   "Fisher-Kolmogorov equation." <u>Wikipedia</u>. 28 Feb. 2014. Wikimedia Foundation. 02
Apr. 2014 <http://en.wikipedia.org/wiki/Fisher-Kolmogorov_equation>.

[18]   "MUltifrontal Massively Parallel sparse direct Solver." <u>MUMPS : A parallel sparse
direct solver</u>. 02 Apr. 2014 <http://mumps.enseeiht.fr/>.

[19]   "Verify and Optimize your designs with COMSOL Multiphysics." <u>COMSOL
Multiphysics®</u>. 02 Apr. 2014 <http://www.comsol.com/>.

[20]   Robinson, K. R. "The Responses of Cells to Electrical Fields: A Review." *The Journal of
Cell Biology* 101 (6), p. 2023, 1985.